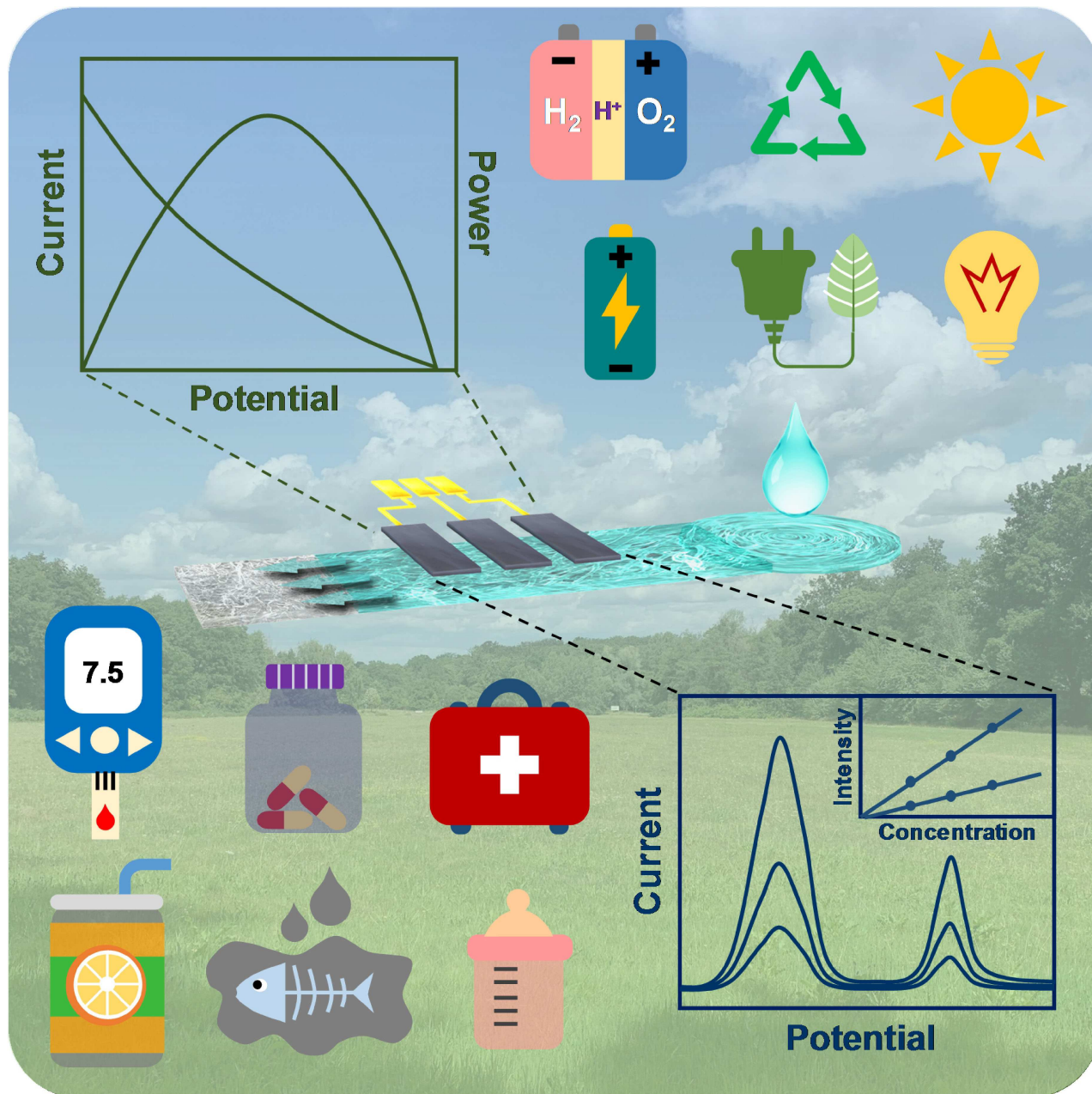


# Paper-Based Microfluidics for Electrochemical Applications

Liu-Liu Shen, Gui-Rong Zhang,\* and Bastian J. M. Etzold\*<sup>[a]</sup>



Paper-based microfluidics is characteristic of fluid transportation through spontaneous capillary action of paper and has exhibited great promise for a variety of applications especially for sensing. Furthermore, paper-based microfluidics enables the design of miniaturized electrochemical devices to be applied in the energy sector, which is especially attractive for the rapid growing market of small size disposable electronics. This review gives a brief summary on the basics of paper chemistry and

capillary-driven microfluidic behavior, and highlights recent advances of paper-based microfluidics in developing electrochemical sensing devices and miniaturized energy storage/conversion devices. Their structural features, working principles and exemplary applications are comprehensively elaborated and discussed. Additionally, this review also points out the existing challenges and future opportunities of paper-based microfluidic electronics.

## 1. Introduction

The emergence of the first microfluidic device dated back to 1979, when a miniaturized gas chromatograph consisting of a capillary column, a sample injection system and a thermal conductivity detector was constructed on a silicon wafer for gas sensing by Terry et al.<sup>[1]</sup> In the 1990s, microfluidics was investigated as possible field-deployable systems for chemical/biological detections.<sup>[2]</sup> Ever since then, microfluidic devices (or lab-on-chips), featuring precise manipulation of fluid at sub-millimeter level, reduced sample consumption, rapid response, and miniaturized size, have attracted intensive research attention.<sup>[2–7]</sup> However, several inherent drawbacks of conventional microfluidic devices including high cost of substrate materials, pumps and pressure control units, along with the complicated fabrication processes have greatly restricted their miniaturization and broad-based applications.

A pioneering solution was proposed by Whitesides et al. in 2007, by reporting the first microfluidic paper-based analytical device ( $\mu$ PAD) for simultaneous detection of glucose and protein using cellulose paper as a substrate.<sup>[20]</sup> This inexpensive, low-volume, portable diagnostic device was based on a patterned paper, where hydrophilic channels were created by building hydrophobic “walls” through photolithography of photoresist. Compared with those traditional substrate materials (e.g., silicon, glass, plastic), paper features abundance, lightness, flexibility, and biodegradability besides its extremely low cost. The inherent abundant micro/nanoscale channels endow paper to transport liquid via capillary actions.<sup>[21–22]</sup> Therefore, pumps which are prerequisite in conventional microfluidics can be eliminated, making the miniaturization of the devices more feasible for real applications. Besides, versatile properties of paper, e.g., thickness, porosity, roughness, and wettability, make it possible to precisely regulate the microfluidic behavior to meet various requirements. After the bench-

mark work from Whitesides et al., various  $\mu$ PADs were developed to implement clinical diagnosis, pharmaceutical industry, environmental monitoring and food safety inspection. Combining paper with microfluidic concept represents a cornerstone for the microfluidic concept, making it possible to fulfill the early promise of microfluidics which fails to be realized on traditional microfluidics.<sup>[23–24]</sup>

Another cornerstone comes when paper-based microfluidics is combined with electrochemical techniques. The early  $\mu$ PADs mainly employ optical methods (e.g., colorimetric, fluorescence). The analyses are realized by visually comparing the color change of the reaction spots before and after loading analytes. The analyte concentration can be quantified using a smartphone camera (installed with image analysis software) or handheld optical colorimeter.<sup>[25–30]</sup> Later on, electrochemical detection methods become widely investigated due to their high detection sensitivity and low limit of detection (LOD) at low cost.<sup>[31–32]</sup> The electrodes can be easily miniaturized and fabricated on paper, and handheld potentiostats have already been widely available for on-site analysis.<sup>[33–36]</sup> The detection properties (e.g., selectivity) can also be well adjusted by varying electrochemical parameters and/or electrode materials for different applications.

Combining paper-based microfluidics with electrochemical techniques also opens a new door to build miniaturized devices for applications in the energy sector. The rapid advance of internet of things (IoT) has spurred the explosive market growth for portable and disposable electronic devices, which are expected to provide multiple functions such as diagnosis, display and sensing. Nevertheless, this also raises the concerns about how to mitigate the power needs of these devices. Button cells, especially lithium-ion batteries (LIBs), are the most widely used power supplies for these disposable devices.<sup>[37–38]</sup> However, the disposal of these devices along with almost fully charged batteries after single use causes energy waste and environment pollution.<sup>[19,38–39]</sup> Therefore, there's an increasing demand to develop miniaturized and green power sources, which can not only be integrated into electronics, but also have minimum environmental impact. To this end, paper-based microfluidics holds great promise to suit this purpose. A pioneering work was performed by Esquivel et al. by reporting the first paper-based microfluidic fuel cell.<sup>[19]</sup> Inspired by this success, many other paper-based microfluidic energy devices (fuel cells, batteries) have been constructed. They are featuring low-cost, lightweight and environmental benign nature, making them ideal substitution of button cells.

[a] L.-L. Shen, Dr. G.-R. Zhang, Prof. B. J. M. Etzold  
Ernst-Berl-Institut für Technische und Makromolekulare Chemie,  
Department of Chemistry,  
Technische Universität Darmstadt,  
Alarich-Weiss-Straße 8, 64287 Darmstadt, Germany  
Fax: +49 6151 1629982  
E-mail: g.zhang@tc1.tu-darmstadt.de  
etzold@tc1.tu-darmstadt.de

 ©2019 The Authors. Published by Wiley-VCH Verlag GmbH & Co. KGaA.  
This is an open access article under the terms of the Creative Commons  
Attribution Non-Commercial NoDerivs License, which permits use and  
distribution in any medium, provided the original work is properly cited, the  
use is non-commercial and no modifications or adaptations are made.

Considering that there are many excellent reviews concerning paper manufacture/fabrications,<sup>[40–42]</sup> paper-based microfluidic devices for sensing/diagnosing,<sup>[43–46]</sup> and electronics using paper substrate (paper electronics),<sup>[21–22]</sup> the current review will mainly focus on the recent advances of paper-based microfluidic concept in electrochemical applications, as shown in Figure 1. The purpose is to summarize some basics and unique features of paper-based microfluidics, and to show how the properties of paper can be used to regulate the electrochemical performance of the resultant devices by highlighting some exemplary applications. Additionally, some critical point of views as well as future outlook and challenges for paper-based microfluidic electrochemical devices will be given.

## 2. Basics of Paper-Based Microfluidics

### 2.1. Paper Chemistry

Paper is usually made by pressing together cellulose fibers,<sup>[22]</sup> which can be separated from raw sources such as wood, cotton and other plants by chemical/mechanical pulping. As the major component of paper, cellulose is a polysaccharide consisting of a linear chain of glucose units linked through  $\beta$ -1,4-glycosidic bonds.<sup>[47]</sup> Cellulose chains are grouped with each other through hydrogen bond to form elementary fibrils, with both crystalline and amorphous regions.<sup>[21,48]</sup> Elementary fibrils aggregate to form 3D microfibrils, and thousands of microfibril bundles bonded together to form the cellulose fiber (Figure 2).<sup>[48–49]</sup> The cellulose fibers are cross-stacked and interconnected during the paper manufacture process, resulting in hierarchical porous structure of paper.<sup>[22]</sup> Thus, paper is considered as an elegant matrix offering a thin mechanically stabilized film of water or other fluids that can deliver analyte/electrolyte to electrode

surfaces, making it an ideal substrate for the portable/disposable electrochemical devices.<sup>[50]</sup>

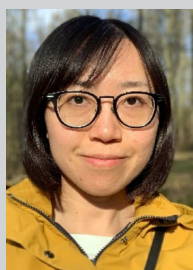
### 2.2. Microfluidics on Paper

Microfluidics is a technology that fluid flow is manipulated in submillimeter level (1–1000  $\mu\text{m}$ ) at least in one dimension. Fluids in a microfluidic system usually feature a low Reynold's number (i.e., laminar flow), i.e., turbulent mixing is minimized and the only mechanism for mixing is diffusion.<sup>[51]</sup> Traditional microfluidic processes take place in channels with dimensions of tens and hundreds of micrometers fabricated by molding, photolithography or etching of a substrate. The flow in a microfluidic channel is usually driven/regulated by a pump.<sup>[52]</sup> Compared with conventional microfluidic systems, paper materials, made of cellulose fibers with hierarchical porous structure, provide a low-cost and pump-less alternative to generate microfluidics through capillarity. The Reynold's number of flow within paper matrix is at the order of  $10^{-3}$ , indicating a typical laminar flow behavior,<sup>[23,53]</sup> which is described by Lucas-Washburn equation:<sup>[54]</sup>

$$x(t) = \sqrt{\frac{\sigma r \cos \theta}{2\eta}} t \quad (1)$$

where  $x$  is the distance moved by the fluid front (m) under capillary pressure,  $\sigma$  is the liquid-air surface tension (N/m),  $t$  is the time (s),  $r$  is the average pore radius of the paper (m),  $\theta$  is the liquid-fiber contact angle, and  $\eta$  is the viscosity (Pa·s). According to the Lucas-Washburn equation, flow velocity ( $v$ ) of liquid in a rectangular paper strip diminishes with time.

The imbibition behavior of fluid deviates from the classic Lucas-Washburn law ( $v \propto t^{-1/2}$ ) when the paper substrate is in



Liu-Liu Shen received her B.S. degree in chemistry from Shandong University in 2012. She obtained her M.S. degree from Department of Chemistry at Tsinghua University in 2016. She is pursuing her Ph.D. degree under the supervision of Prof. Etzold at Technische Universität Darmstadt funded by China Scholarship Council. Her research mainly focuses in the development of paper-based microfluidic electronics for fast analysis and portable power supply. She also carries research on synthesis of functional carbon materials, polymer electrolyte membrane fuel cell and metal-air battery.



Dr. Gui-Rong Zhang received his B.S. degree from Beijing University of Chemical Technology in 2007. He obtained his Ph.D. from Tsinghua University in 2013. After a short stay at Institute of Metal Research (CAS), he moved to Germany working with Prof. Etzold as a postdoc at University of Erlangen-Nürnberg and then Technische Universität Darmstadt. Now he is a group leader of electrochemistry.



His research focuses on development of metal- or carbon-based nanomaterials for electrochemical applications including fuel cells, batteries, electrosyntheses and paper-based microfluidics.

Prof. Bastian J. M. Etzold obtained his PhD at Universität Bayreuth in 2007, and later joined Cluster of Excellence "Engineering of Advanced Materials (EAM)" at University of Erlangen-Nürnberg. In 2010 he was appointed as junior professor within EAM Rising Star Program. In 2011 he joined for 6 months Prof. Gogotsi's group (Drexel University) through Alexander-von-Humboldt fellowship. From 2015, he is a full professor at Technische Universität Darmstadt. His current research focuses on new processes and materials for synthesis and use of energy carriers and base chemicals.

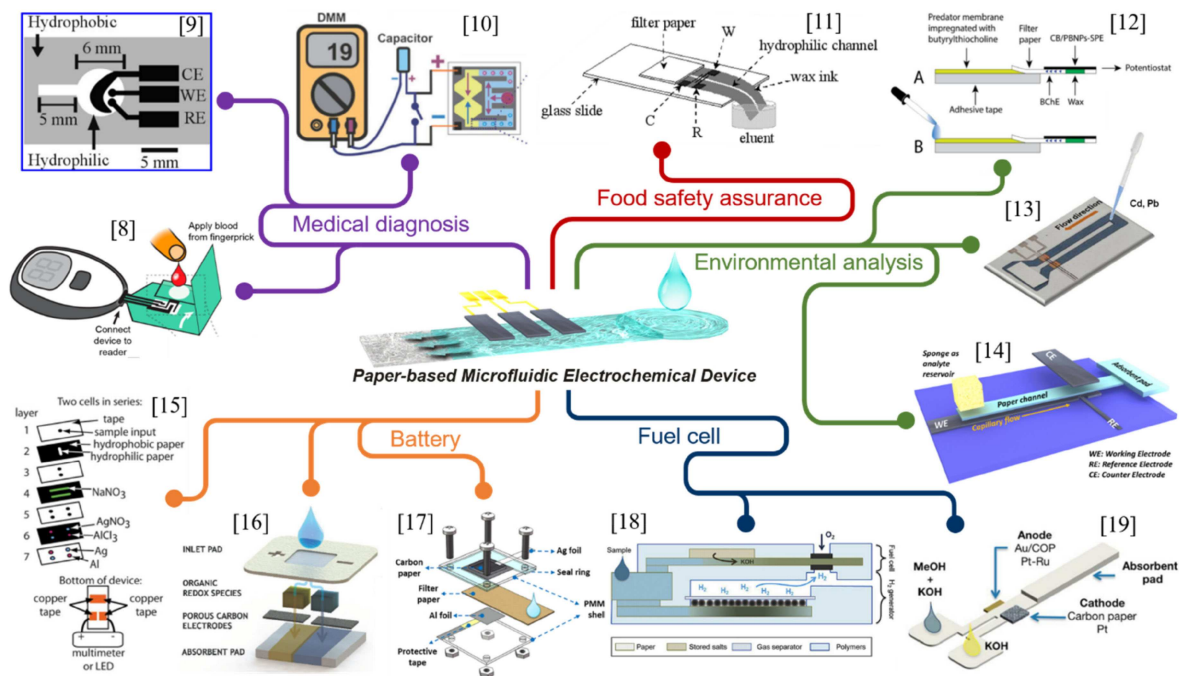


**Figure 1.** Overview of typical applications of paper-based microfluidic electrochemical devices. Reprinted with permission.<sup>[8]</sup> Copyright 2016 American Chemical Society. Reprinted with permission.<sup>[9]</sup> Copyright 2009 American Chemical Society. Reprinted with permission.<sup>[10]</sup> Copyright 2012 Wiley-VCH. Reprinted with permission.<sup>[11]</sup> Copyright 2013 Wiley-VCH. Reprinted with permission.<sup>[12]</sup> Copyright 2017 Elsevier. Reprinted with permission.<sup>[13]</sup> Copyright 2015 Springer. Reprinted with permission.<sup>[14]</sup> Creative Commons license 4.0 (CC BY-NC-ND 4.0). Reprinted with permission.<sup>[15]</sup> Copyright 2012 Royal Society of Chemistry. Reprinted with permission.<sup>[16]</sup> Creative Commons license 4.0 (CC BY-NC 4.0). Reprinted with permission.<sup>[17]</sup> Copyright 2019 Elsevier. Reprinted with permission.<sup>[18]</sup> Copyright 2017 Elsevier. Reprinted with permission.<sup>[19]</sup> Creative Commons license 3.0 (CC BY 3.0).

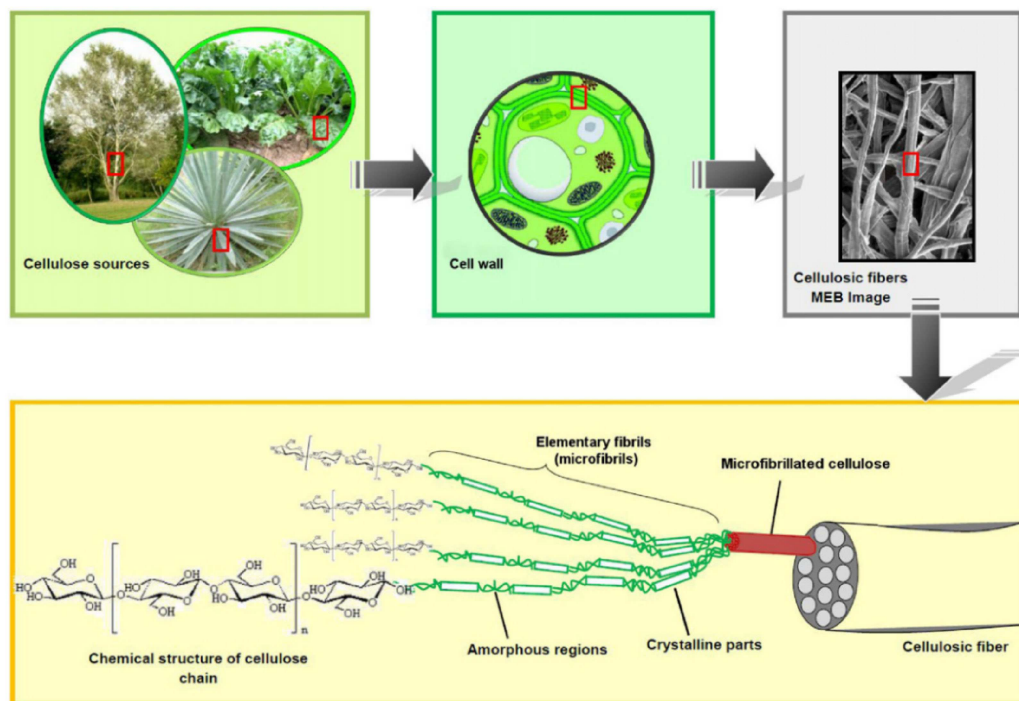


**Figure 2.** Scheme of the hierarchical structure of cellulose fibers. Reprinted with permission.<sup>[49]</sup> Copyright 2012 Elsevier.

different geometry.<sup>[55–57]</sup> Mendez et al. investigated the imbibition behavior of lateral flow on rectangular membrane appended to circular sectors, and showed that a continuous

increase in unwetted pore volume causes a deviation from traditional imbibition, and leads to quasi-stationary flow ( $v \propto t^0$ ) in the rectangular element.<sup>[56]</sup> In the fabrication of microfluidic

electronics, flow with a constant velocity is usually more preferable, since electrochemical responses might be sensitive to the flow rate of electrolyte. Besides changing the geometry of the porous substrate, another more straightforward method to obtain a stationary flow is to incorporate absorbent pads.<sup>[37,58]</sup>

Devices combining multiple functions with self-power units show the need for transporting different fluids on different pathways. When fabricating such multiplex devices using paper, multiple inlets are usually needed. Various fabrication techniques have been developed for this purpose, mainly including wax-printing (e.g., screen-printing, wax-dipping/impregnation), 2D shaping/cutting (e.g., knife plotter, CO<sub>2</sub> laser cutting), and 3D packaging/stacking (e.g., origami). Moreover, some laboratory-scale methods such as photolithography, PDMS printing, inkjet etching, printed circuit, and plasma/laser treatment, have also been developed to fabricate paper microfluidics, while these methods may not be suitable for large-scale production due to their tedious procedure and high cost. These 2D or 3D methods are supposed to enable efficient transport of fluids in both horizontal and/or vertical dimensions.<sup>[59]</sup>

For instance, Yager et al. reported a two-dimensional paper networks with multiple inlets.<sup>[23,60–62]</sup> The fluid flow behavior is complicated by the interplay between advection flow rate and diffusive mixing rate of the inlet streams. As shown in Figure 3a, two dye solutions flow in parallel on a Y shaped paper channel, and a clear boundary can be observed between these two streams. The boundary position can be readily controlled by adjusting the inlet length ratio. Shen et al. studied the influence of paper texture on the interface of bi-laminar flow on Y-shaped paper, and found that broader diffusion zone was obtained on paper with smaller pore size (Figure 3b).<sup>[37]</sup>

A further advancement toward more complex devices are paper-based microfluidics with 3D configurations. Figure 4a shows a Y-mixer fabricated by stacking two paper channels to maximize the diffusion interface and reduce diffusion distance.<sup>[23]</sup> A paper diluter is designed based on the same mechanism (Figure 4b), and the dilute factor can be tuned by varying lengths of the diluent and main channels.<sup>[23]</sup> Moreover, it is also demonstrated that within a 3D-setup constructed by stacking one piece of paper (overlay channel) onto the other piece (main channel), the flow patterns of liquids in both channels are synchronized (Figure 3c).<sup>[58]</sup> Therefore, the over-

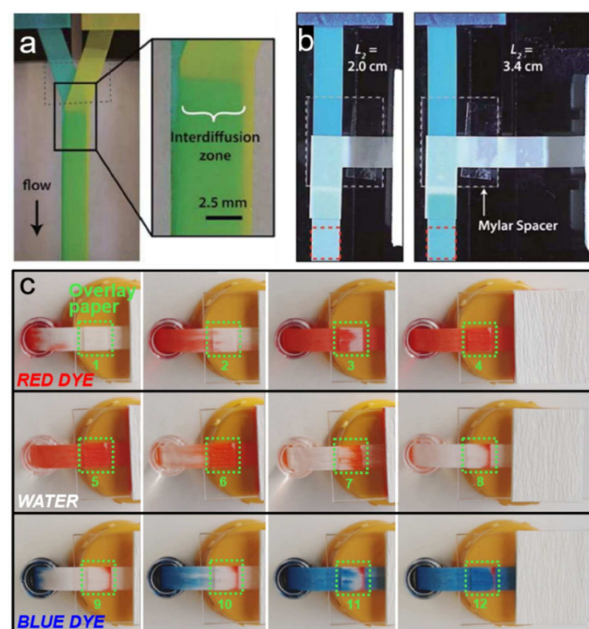


**Figure 4.** (a) Mixing process in a 3D flat Y-mixer. Inlets contain erioglaucine (left) and tartrazine (right). (b) A paper diluter with the top inlet containing erioglaucine, and the right inlet as diluent (H<sub>2</sub>O). Two different diluent arm lengths result in different dye concentrations in the outlets. Reprinted with permission.<sup>[23]</sup> Copyright 2010 Royal Society of Chemistry. (c) Flow patterns of dye solutions within the main paper channel and overlay paper (marked with green square). Reprinted with permission.<sup>[58]</sup> Creative Commons license 3.0 (CC BY-NC 3.0).

layer can be flexibly used to construct reaction zone with catalyst or enzyme to meet different application requirements such as power generation or analysis.

Besides flow rate control and multi-flow construction, programming of fluid flow can also be achieved on paper without any external equipment.<sup>[40]</sup> As shown in Figure 5a, the fluid flow rate can be easily regulated using strips with different width.<sup>[61,63]</sup> A dissolvable barrier can be used to delay the transport of fluid on paper (Figure 5b).<sup>[61]</sup> Tunable-delay shunts for paper microfluidics can also be realized using absorbent pads (Figure 5c).<sup>[64]</sup> More sophisticated multi-fluid transport can also be programmed on paper.<sup>[60–61]</sup> As shown in Figure 5d, three reagents can be delivered sequentially to the “detection

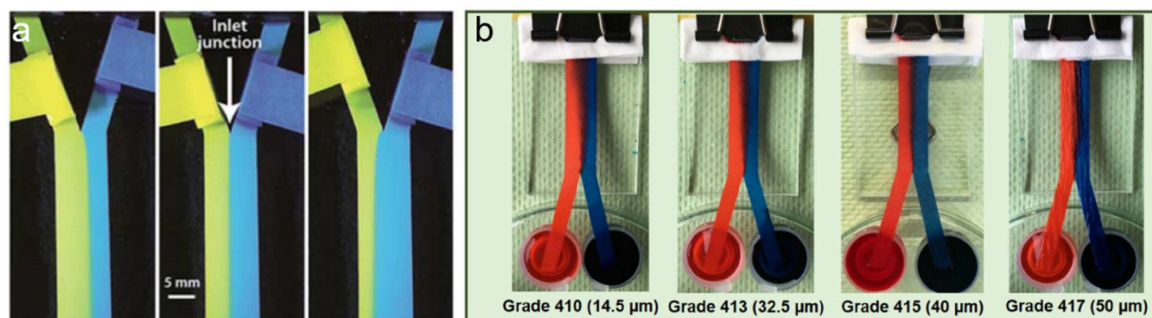


**Figure 3.** Demonstration of flow control by varying inlet arm lengths in Y-shaped paper strips. Reprinted with permission.<sup>[23]</sup> Copyright 2010 Royal Society of Chemistry. (b) Cross diffusion of bi-laminar flow on different Y-shaped paper strips. Reprinted with permission.<sup>[37]</sup> Copyright 2019 Elsevier.

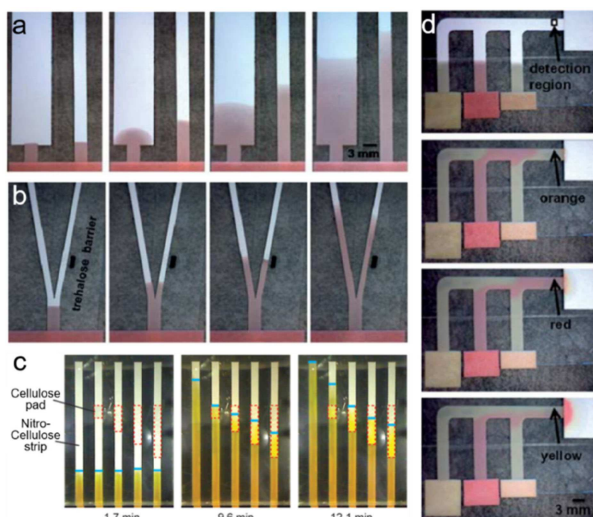


**Figure 5.** (a) Dependence of the flow rate on the width of paper strips. (b) A dissolvable barrier on the right delays the fluid transport. Reprinted with permission.<sup>[61]</sup> Copyright 2010 Royal Society of Chemistry. (c) Time-lapse images of the flow through nitrocellulose strips. Reprinted with permission.<sup>[58]</sup> Copyright 2013 American Chemistry Society. (d) The programmed fluid delivery using a 2D paper network. Reprinted with permission.<sup>[61]</sup> Copyright 2010 Royal Society of Chemistry.

region" with three staggered inlets connected to the main channel.<sup>[61]</sup>

Based on these reports, it can be seen that precise control of microfluidic flow on paper, including flow rate, multi-channel flows, mixing/dilution, and programming/timing can be realized without expensive external control system or power supply, which provides the basis for the various applications of paper microfluidics. The porosity and flexibility of paper enable researchers to construct microfluidic channels and electrochemical reaction zones by well-established techniques, such as wax-printing, screen-printing, origami, cutting and stacking. Thus, paper-based microfluidics provides a versatile platform to construct low-cost miniaturized electronics with various functionalities toward practical applications as detailed in the following context.

### 3. Electrochemical Sensing Devices

Paper-based microfluidic electrochemical devices have attracted growing interest in the field of sensing, due to their low cost, flexibility, disposability, high sensitivity and ability to perform diverse measurements. Table 1 summarizes some typical paper-based microfluidic electrochemical sensing devices for various applications, e.g., medical diagnosis, environmental monitoring and food safety assurance, along with their components, fabrication methods, performance and general features. As shown in Table 1, Whatman grade 1 chromatography paper appears to be the most-used paper in fabricating the paper-based microfluidic electrochemical sensing devices, because it is commercially available, easy to be modified and exhibits

good wicking properties.<sup>[42]</sup> More detailed information will be given in the following content.

#### 3.1. Medical Diagnosis

Point-of-care (POC) diagnosis is essential in disease prevention and treatment. The goal of POC applications is to provide an answer when a sample is introduced to the device and readout is generated that can be used to make an informed decision.<sup>[9]</sup> Therefore, affordable, user-friendly, rapid and sensitive diagnostic sensors are always highly demanded. Paper-based microfluidic electrochemical sensors have attracted intensive research interest in the field of POC diagnosis due to their low cost, flexibility, disposability, high sensitivity and capability to perform diverse measurements.

Dungchai et al. developed the first microfluidic paper-based electrochemical device ( $\mu$ PED) in 2009 for detecting glucose, lactate and uric acid in biological samples.<sup>[9]</sup> As shown in Figure 6a, the  $\mu$ PED consists of microfluidic channels on filter paper patterned by photolithography and screen-printed electrodes. When the analyte flows through the three electrode zones, the corresponding oxidase enzymes catalyze the relevant oxidation reactions. Amperometric current is recorded for quantitative analysis with Prussian Blue (PB) as a redox mediator. With such a simple device, rather low LODs for glucose and lactate (shown in Table 1) can be achieved, being sufficient for clinical diagnosis. This work demonstrates for the first time the feasibility of fabricating electrochemical analytical devices using paper microfluidic concept. Moreover, this pioneering work also provides the basis of device configurations and working principles, which have been widely adopted by many follow-up works on developing  $\mu$ PED for analytic applications.

Almost at the same time, Nie et al. presented a similar  $\mu$ PED by screen-printing electrodes on paper/polyester film which was attached to paper-based microfluidic channels (Figure 6b).<sup>[73]</sup> The  $\mu$ PEDs are compatible with the commercially available hand-held glucometer. After placing a drop of analyte solution in the detection zone, the glucometer will display the results based on amperometric measurements. A number of compounds concerning human health (e.g., glucose, cholesterol, lactate and alcohol) can be quantified on the  $\mu$ PEDs. One of the most appealing features of this work is that the  $\mu$ PEDs are compatible with a user-friendly glucometer, and thus the readout can be easily achieved without using any potentiostat which is not commonly available in people's daily life. However, the detection accuracy still needs to be improved when comparing to conventional glucometers. Regarding improving the sensing performance of  $\mu$ PEDs, an interesting attempt was made by Li et al., who fabricated a  $\mu$ PED using zinc oxide nanowires (ZnO-NWs) decorated working electrode for glucose detection (Figure 6c).<sup>[66]</sup> The resulting  $\mu$ PED exhibits higher sensitivity and lower LOD (59.9  $\mu$ M) than a commercial glucometer. The superior performance of the ZnO-NWs modified  $\mu$ PED is attributed to the large surface area and their strong electrostatic attraction with the glucose oxidase of ZnO-NWs,

**Table 1.** Summary of the typical paper-based microfluidic electrochemical sensing devices.

Working electrode or reaction area	Fabrication method	Analysis method <sup>[a]</sup>	Paper type (flow rate)	Analyte and corresponding LOD <sup>[b]</sup>	Features	Ref.
PB <sup>[c]</sup> /carbon modified with enzyme	Photolithography, screen-printing	CA	Whatman grade 1	Glucose: 0.21 mM Lactate: 0.36 mM Uric acid: 1.38 mM	The first microfluidic paper-based electrochemical device	[9]
Carbon, enzyme	Photolithography, screen-printing	CA	Whatman grade 1	Glucose: 0.22 mM	Compatible with a commercial glucometer	[65]
ZnO NWs <sup>[d]</sup> on carbon	Wax-printing, stencil-printing	CA	Whatman grade 1	Glucose: 59.5 μM	Low LOD achieved by electrode modification	[66]
Aptamers, glucose oxidase labeled DNA	Wax-printing, screen-printing, origami	CC	Whatman grade 1	Adenosine: 11.8 μM	Self-powered sensor	[10]
Carbon, antibodies mobilized on MWCNTs <sup>[e]</sup>	Wax-printing, screen-printing, origami	DPV	Not mentioned	AFP <sup>f</sup> : 0.01 ng/mL CA125 <sup>g</sup> : 6.0 mU/mL CA199 <sup>g</sup> : 8.0 mU/mL CEA <sup>g</sup> : 5.0 pg/mL	Highly integrated for simultaneous detection of 4 cancer markers	[67]
Carbon, antibodies mobilized on CdS NPs <sup>[e]</sup> and MWCNTs <sup>[e]</sup>	Wax-printing, screen-printing, origami	PEC	Whatman grade 1	CEA <sup>g</sup> : 2.1 pg/mL	Multiplex immunoassay based on PEC	[68]
Au	Wax-printing, sputtering	CA	Whatman P81	Paracetamol: 25 μmol/L 4-aminophenol: 10 μmol/L	Efficient separation of analytes by the paper channel	[69]
Carbon, Bi	Photolithography, screen-printing	ASV	Whatman grade 1	Pb <sup>2+</sup> : 1.0 ppb	Enhanced sensitivity with fluidic analyte	[65]
Graphite	Wax-printing, screen-printing	SWV	Whatman grade 1	Cd <sup>2+</sup> : 11 ppb Pb <sup>2+</sup> : 7 ppb	Capable to detect mud-spiked sample	[13]
Graphite foil	Cutting, stacking	SWV	VWR415 (130 μL/min)	Cd <sup>2+</sup> : 1.2 μg/L Pb <sup>2+</sup> : 1.8 μg/L	Modifier-free electrodes	[14]
Ru@AuNPs <sup>[e]</sup> and Si@CNCs <sup>[e]</sup> conjugated DNA strands	Wax-printing, screen-printing	ECL	Whatman grade 1	Pb <sup>2+</sup> : 10 pM Hg <sup>2+</sup> : 0.2 nM	Capable to detect lake water and human serum sample	[70]
Polypyrrole/ZnO/AuNPs <sup>g</sup> /paper	Origami, molecular imprinting	PEC	Whatman grade 1	Pentachlorophenol: 4 pg/mL	Capable to detect real sample	[71]
Carbon black and PB <sup>[c]</sup> NPs, butyrylthiocholine	Wax-printing, screen-printing	CA	Cordenons filter paper, 67 g/m <sup>2</sup>	Paraoxon: 10 μg/L	Reagent-free analysis	[12]
Pencil stroke	Wax-printing, pencil-drawing	CA	Whatman grade 1	Ascorbic acid: 30 μM Sunset yellow: 90 μM	Efficient separation of analytes by the paper channel	[11]
Carbon	Ink-writing	DPV	A4 paper 70 mg	Melamine: 1.0 μM	Easy fabrication by writing electrodes on paper	[72]

[a] CA: chronoamperometry; CC: concentration cell; DPV: differential pulse voltammetry; ASV: anodic stripping voltammetry; SWV: square wave voltammetry; ECL: electrochemiluminescence; PEC: photoelectrochemistry. [b] LOD: Limit of detection [c] PB: Prussian Blue; NWs: nanowires; NPs: nanoparticles; MWCNTs: multi-wall carbon nanotubes; Ru@AuNPs: Ru(bpy)<sub>3</sub><sup>2+</sup> gold nanoparticles aggregates; Si@CNCs: carbon nanocrystals capped silica nanoparticles; AFP: f-fetoprotein; CA125: carcinoma antigen 125; CA199: carcinoma antigen 199; CEA: carcinoembryonic antigen; AuNPs: gold nanoparticles.

which favors a stable and efficient immobilization of enzymes. This work demonstrates that surface modifier on the working electrode can be employed as a handle to improve the sensing performance of μPEDs.

To meet the requirement of high-throughput diagnosis using μPED, Zhao et al. presented a paper-based electrochemical biosensor array for multiplexed detection of physiologically relevant metabolic biomarkers.<sup>[34]</sup> As shown in Figure 6d, the device includes an array of eight microfluidic electrochemical paper-based sensors. The reaction zone in each sensor is modified with the corresponding enzyme for detecting different metabolic biomarkers. Combined with a handheld custom-made multi-channel potentiostat, the biosensor array can be used to perform multiple measurements from a single run, giving the quantification results of glucose, lactate and uric acid in artificial urine. The device performance is reported to be comparable to that of the existing commercial meters, meeting

the clinically relevant levels of all three markers in urine. This work provides a promising solution to achieve high-throughput analyses by combining multiple μPEDs with a cheap portable multi-channel potentiostat, while the interpretation of the readout from a potentiostat may still be a challenging task for regular users without proper training, which may represent a major barrier for this platform to penetrate the market.<sup>[74]</sup>

There is some exciting progress in fabricating μPEDs with 3D configuration, usually composing of multiple layers with different functions and/or capability to simultaneously detect multiple analytes.<sup>[42,76]</sup> 3D network of paper devices can be fabricated by either stacking or folding (origami). For instance, Liu et al. proposed a 3D origami paper analytical device (oPAD) for adenosine detection.<sup>[10]</sup> As illustrated in Figure 7a, the inlet, microfluidic channels connected with two half-cells are accommodated on one piece of paper, while the electrodes are printed on another piece. After folding and laminating, the

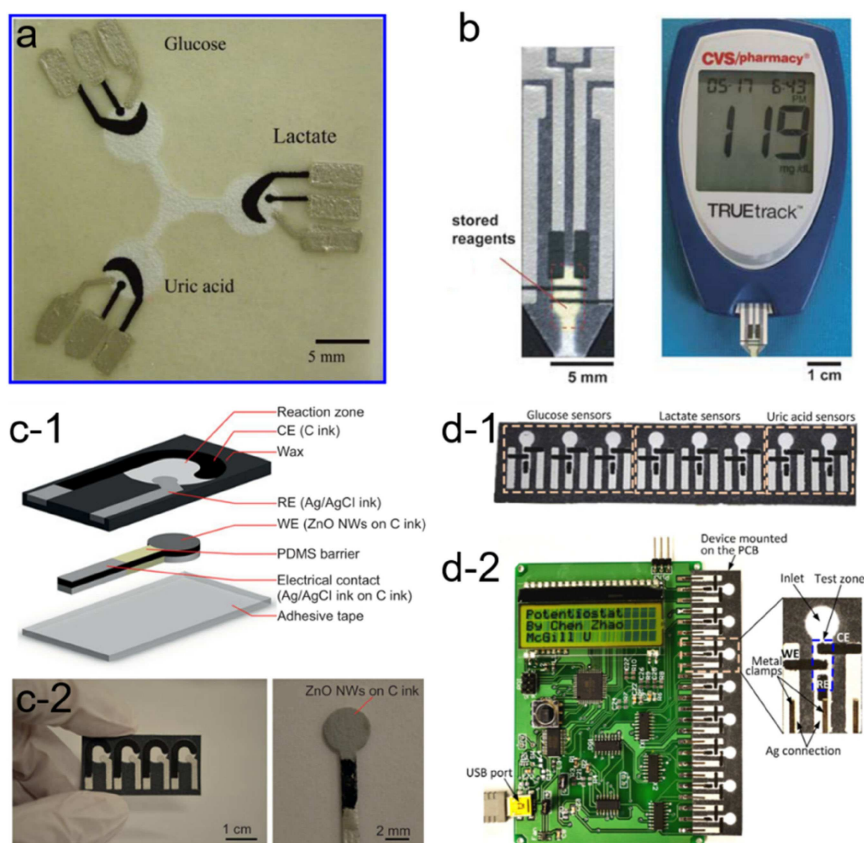


**Figure 6.** (a) A  $\mu$ PED for detection of glucose, lactate and uric acid. Reprinted with permission.<sup>[9]</sup> Copyright 2009 American Chemical. (b) A  $\mu$ PED made from a single layer of paper (left) and a glucometer (right). Reprinted with permission.<sup>[73]</sup> Copyright 2010 Royal Society of Chemistry. (c) Schematic of ZnO-NWs  $\mu$ PED (c-1), an array of  $\mu$ PEDs (c-2, left), and a working electrode with ZnO NWs grown over its circular area (c-2, right). Reprinted with permission.<sup>[66]</sup> Creative Commons license 4.0. (d) A microfluidic paper-based electrochemical biosensor array (d-1) that interfaces with a custom-made handheld potentiostat (d-2) for multiplexed detection of metabolic biomarkers. Reprinted with permission.<sup>[34]</sup> Creative Commons license 3.0.

electrodes are right underneath these two half-cells. Analyte is added at the inlet, and then split into the two channels. The reaction between adenosine and modifier in the experimental channel causes ion concentration change in one half-cell, and the difference in the concentrations of ions in the two half-cell results in a voltage, which is used to charge a capacitor. The quantification is implemented by measuring the discharging current of the capacitor using a multimeter. The high instantaneous current provided by the capacitor results in much higher sensitivity than those conventional methods (Figure 7b). The oPAD can generate current without using external power sources. The sensing process can be simply operated with a commercially available multimeter, and the readout is easy to interpret. By choosing proper modifiers, the oPAD is capable to become a sensing platform for many other biomarker detections.

Yu et al reported a series of microfluidic paper-based electrochemical immunodevices ( $\mu$ PEIDs) based on origami technique, which are capable for multiplex analyses.<sup>[67,77–78]</sup> Figure 7c shows a 3D- $\mu$ PEID consisting of two stacked layers of wax-patterned square papers. In this configuration, eight working electrodes share the same reference and counter electrodes.<sup>[67,77]</sup> This unique design allows multi-detection to be

carried out simultaneously, which not only increases the detection efficiency but also offers another approach to realizing high-throughput analyses. A typical horseradish peroxidase-O-phenyl-eneidamin- $\text{H}_2\text{O}_2$  electrochemistry system is adopted as the detection strategy. Four cancer markers, r-fetoprotein, carcinoma antigen 125, carcinoma antigen 199 and carcinoembryonic antigen were detected on the 3D- $\mu$ PEID (Figure 7d). The linear ranges and LODs of these cancer markers cover most of the levels in human plasmas and serums. The same group also presented a high-performance electrochemical DNA sensor based on the 3D- $\mu$ PEID.<sup>[78]</sup> Wu et al. introduced signal amplification strategy to  $\mu$ PEIDs for multiplexed detection of cancer biomarkers, which significantly enhanced the sensitivity of the device.<sup>[79–80]</sup> Moreover,  $\mu$ PADs based on photoelectrochemical (PEC) and electrochemiluminescence (ECL) methods are also developed for diagnostic applications especially in the field of immunoassay.<sup>[68,81–88]</sup> The pioneering work was conducted by Wang et al, who reported for the first time an origami PEC-based  $\mu$ PAD for cancer marker (CEA) detection. By employing a paper supercapacitor as an amplifier, the photocurrent signal can be largely increased, resulting in a low LOD.<sup>[68]</sup>

Besides fabricating  $\mu$ PEDs with 3D configuration, another approach to realizing multiplex analyses is to take the

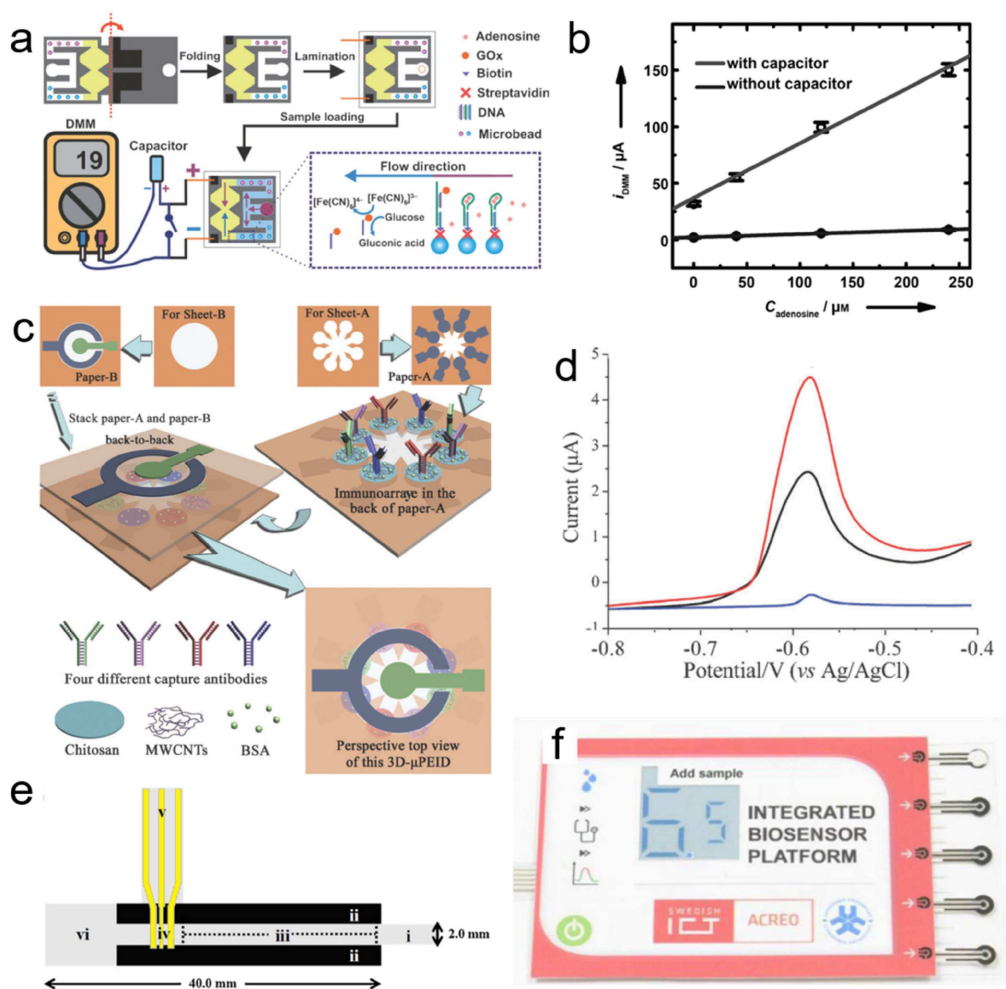


**Figure 7.** (a) The operating principle of the aptamer-based oPAD. (b) Calibration curves for detecting adenosine with and without amplification by capacitor. Reprinted with permission.<sup>[10]</sup> Copyright 2012 Wiley-VCH. (c) Scheme of fabricating the 3D- $\mu$ PEID. (d) Differential pulse voltammetric curves of carcinoembryonic antigen (CEA) as a model (blue line: background; black line: 0.25 ng/mL CEA; red line: 1.5 ng/mL CEA). Reprinted with permission.<sup>[67]</sup> Copyright 2012 Royal Society of Chemistry. (e) Scheme of the paper-based microfluidic device for separation and electrodedetection of paracetamol and 4-aminophenol. Reprinted with permission.<sup>[69]</sup> Copyright 2012 Elsevier. (f) Photograph of the integrated instrument for glucose detection. Reprinted with permission.<sup>[75]</sup> Copyright 2015 Electrochemical Society.

advantage of paper chromatography in separating different analyses. Shiroma et al. constructed a simple low-cost  $\mu$ PED for detecting paracetamol and 4-aminophenol.<sup>[69]</sup> The device consists of a paper microfluidic channel and Au electrodes (Figure 7e). The hydrophilic channel on the paper serves as a low-cost separation platform. The separated 4-aminopheno and paracetamol are detected at the electrode zone in the end of the paper channel in sequence, and possible interference from different analytes can be minimized.

Despite the great success in developing various  $\mu$ PEDs to fulfill different diagnostic purposes, quite few of them has really penetrated the market. In the field of glucose-monitoring,  $\mu$ PEDs that are compatible to commercial glucometer hold great potential for marketing, as demonstrated in the benchmark work of Whitesides et al. in 2010, while better flow control might represent one of the major obstacles for their commercialized applications.<sup>[89]</sup> So far,  $\mu$ PED system that is the closest to practical application is demonstrated by Acreo Company

(Sweden), who presented an entire glucose detection system equipped with battery, microfluidic sensor and electrochromic display unit on a piece of plastic or paper (Figure 7f).<sup>[75,90–91]</sup> However, the printed circuits still base on silicon chip and conventional alkaline battery, which inevitably increases cost and may cause environmental pollution. It is envisioned that in the future  $\mu$ PEDs can be fabricated mainly by paper materials, using paper-based power supplies, the development of which will also be presented later.

### 3.2. Environmental Monitoring

Environmental pollution is one of the major problems that effects ecosystem and human health worldwide. Conventional laboratory techniques, such as atomic absorption spectroscopy, X-ray fluorescence spectroscopy and inductively coupled plasma mass spectroscopy are broadly used in environmental

monitoring and analyses, presenting low LOD and high sensitivity. However, the above-mentioned techniques are fixed-site laboratory analysis which rely on expensive equipment, tedious sample preparation and high-skilled technicians. This limits their application for on-site analysis, especially in some developing areas with insufficient infrastructures.<sup>[44,50,92–93]</sup> Portable, low-cost, user-friendly, rapid and sensitive sensing devices are therefore highly desired by the market.  $\mu$ PEDs featuring low price, high sensitivity and selectivity, wide linear range, miniaturized in size and minimal power requirements emerge as an attractive platform for rapid on-site monitoring of environmental pollution.<sup>[94]</sup>

As a typical environment pollutant, heavy metal ions (e.g.,  $\text{Cd}^{2+}$ ,  $\text{Pb}^{2+}$ ) are toxic, non-biodegradable, and tend to accumulate in plants and animals, thus imposing severe risks to human health.<sup>[13,95–97]</sup> Typical electrochemical detection of heavy metals include two steps: 1) Deposition of heavy metal ions at a negative potential; 2) Anodic stripping heavy metal for quantitative analysis.<sup>[98–100]</sup> This detection is usually carried in a three-electrode cell setup with continuous stirring.<sup>[100–104]</sup> This approach has several drawbacks: 1) it is difficult to minimize the whole setup for on-site measurements;<sup>[65]</sup> 2) the electrochemical cell and the electrodes are expensive, making them not economic feasible for single use.<sup>[50]</sup> To eliminate these drawbacks, a three-electrode system can be fabricated by screen printing electrodes onto a substrate, with analysis being carried out by placing a drop of sample on the three-electrode strip.<sup>[105–107]</sup> However, this approach shows limited sensitivity, because the deposition of the heavy metal is limited by the diffusion in the stagnant sample drop.<sup>[65]</sup>

To this end, Nie et al. employed  $\mu$ PED for heavy metal detection (Figure 8a).<sup>[65]</sup> The  $\mu$ PED comprises paper-based microfluidic channels, and screen-printed electrodes. The  $\mu$ PED is used to selectively detect  $\text{Pb}^{2+}$  in the mixed solution of  $\text{Pb}^{2+}$  and  $\text{Zn}^{2+}$ . Compared with stagnant sample, microfluidic configuration greatly enhances the deposition efficiency and improves the LOD (1.0 ppb). Similarly, Medina-Sanchez et al. proposed a lateral flow paper-based electrochemical sensor for heavy metal detection (Figure 8b).<sup>[13]</sup> A wide linear range from 10 to 100 ppb with low LODs (7 and 11 ppb for  $\text{Pb}^{2+}$  and  $\text{Cd}^{2+}$ , respectively) can be achieved. The device can also be used for mud-spiked

samples, since the paper channel can function as a filter to separate the solution from solid (Figure 8b). However, a proper surface modification on the working electrode is necessary in these electrochemical sensors to promote the deposition efficiency by forming “fuse alloys” with target heavy metals.<sup>[108–110]</sup> This is achieved by using either toxic mercury electrode which makes the device not disposable, or using in situ bismuth modification which complicates the detection process.

In view of this, an innovative  $\mu$ PED platform was proposed by Shen et al. by fabricating a modifier-free microfluidic electrochemical carbon-based sensor ( $\mu$ CS) for heavy metal detection.<sup>[14]</sup> As shown in Figure 8c, the  $\mu$ CS device is based on a microfluidic paper channel combined with a 3D layout with working and counter electrodes facing each other and analyte flowing along the paper channel between these two electrodes. The electrodes are made of entirely by commercial graphite foils, without any surface modifier. LODs down to 1.2  $\mu\text{g/L}$  for  $\text{Cd}^{2+}$  and 1.8  $\mu\text{g/L}$  for  $\text{Pb}^{2+}$  can be achieved on this simple platform. Both metal ions can be simultaneously detected with a linear detection range of 20 to 100  $\mu\text{g/L}$ , and a detection limit of 6  $\mu\text{g/L}$  for both metal ions (Figure 8f). Moreover, this low cost, easy-to-fabricate and modifier free  $\mu$ CS is found to be rather robust, and exhibits good reproducibility over 10 repetitive measurements on a single device, demonstrating great potential for practical applications.

ECL and PEC detections are also introduced to develop  $\mu$ PED for environmental sensing.<sup>[70–71,111]</sup> Yu et al. proposed a 3D paper-based ECL device for simultaneous detection of  $\text{Pb}^{2+}$  and  $\text{Hg}^{2+}$  in lake water and human serum.<sup>[70]</sup> Compared with  $\mu$ PEDs using conventional anodic stripping methods (e.g., DPV and SWV), the 3D ECL  $\mu$ PED exhibits much lower LODs for both  $\text{Pb}^{2+}$  (10 pM) and  $\text{Hg}^{2+}$  (0.2 nM). The same group also developed high-performance paper-based microfluidic origami PEC sensor for S-fenvalerate and pentachlorophenol detection, respectively, both of which are considered as toxic environmental pollutants.<sup>[71,111]</sup>

Cinti et al. reported a fully-integrated reagent-free paper-based electrochemical biosensor for nerve agents (e.g., paraxon) detection in river and industry wastewater.<sup>[12]</sup> The device consists of a strip of a nitrocellulose membrane impregnated

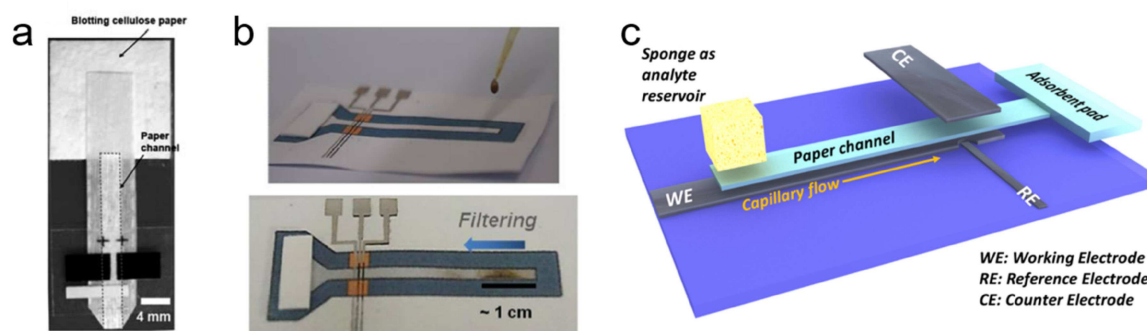


**Figure 8.** (a) A  $\mu$ PED for quantifying heavy metal ions. Reprinted with permission.<sup>[65]</sup> Copyright 2010 Royal Society of Chemistry. (b) The lateral flow paper-based device for heavy metal detection. Reprinted with permission.<sup>[13]</sup> Copyright 2015 Springer. (c) Scheme of the  $\mu$ CS. Reprinted with permission.<sup>[14]</sup> Creative Commons license 4.0 (CC BY-NC-ND 4.0).

with butyrylthiocholine integrated with a paper-based test area that holds a screen-printed electrode and butyrylcholinesterase (BChE) enzyme (Figure 9a). The principle of this approach is based on dual electrochemical measurements of BChE enzyme activity toward butyrylthiocholine with and without the inhibition from the nerve agents. This biosensor gives a linear response with concentration up to 25  $\mu\text{g/L}$  and a LOD down to 3  $\mu\text{g/L}$  (Figure 9b). Moreover, the BChE paper-based electrochemical biosensor also shows the capability to detect organophosphorus and carbamic pesticides.

### 3.3. Food Safety Assurance

Food safety represents another major public health concern.<sup>[112]</sup> A variety of additives, such as sweeteners and food pigments, are widely used in food and beverage industries to improve the taste or color of products, but are usually only allowed to be used at a limited amount. Various  $\mu\text{PEDs}$  have been developed for rapid detection of food additives. Dossi et al. fabricated a simple paper-based electrochemical device (PED) for simultaneous detection of ascorbic acid and sunset yellow, which were frequently found as additives in foodstuffs.<sup>[111]</sup> The PED consists of a pencil-drawn electrode (PDE) detector and microfluidic channels fabricated by wax printing (Figure 9c). These two analytes can be separated and detected in sequence, as reflected by two distinctive peaks on the *i-t* profiles (Figure 9d), and the concentration of the analytes can be quantified according to their peak intensities. Lawrence et al. reported a glucose amperometric sensor, which comprised of a cellulose

paper with immobilized glucose oxidase, placed on top of a screen-printed carbon electrode. The sensor requires only 5  $\mu\text{L}$  of analyte for glucose analysis, and is successfully applied to glucose detection in commercial carbonated beverages with a limit of 0.18 mM.<sup>[113]</sup> Attempts are also made to use  $\mu\text{PEDs}$  for detecting illegal additives in food products, such as melamine which can cause kidney failure but is reported to be illegally added into infant formula to increase the apparent N content. Li et al. developed a  $\mu\text{PED}$  system where the electrodes were directly written onto paper substrate using a syringe filled with carbon ink, and the  $\mu\text{PED}$  could be used to quantify the concentration of melamine in phosphate-buffered saline in presence of uric acid. The working principle is to quantify the reduction in voltammetric oxidation current of uric acid, which is sensitive to the concentration of melamine due to the competition adsorption of melamine and uric acid on working electrode. A wide linear range between 0 to 40  $\mu\text{M}$  and an impressively low LOD (1.0  $\mu\text{M}$ ) can be achieved on this simple  $\mu\text{PED}$ .<sup>[72]</sup>

These exemplary applications indicate that  $\mu\text{PEDs}$  show great promise in the field of sensing. By carefully selecting electrode materials, device configurations and electrochemical methods,  $\mu\text{PEDs}$  can become an innovative and versatile platform for many different sensing applications especially for fast, accurate and on-site analyses. However, most of these  $\mu\text{PEDs}$  still need to be operated with laboratory potentiostat by people with expertise, and sample preparation is necessary before the analysis, which impede them to become commercially available in the real application. This opens the perspective to broaden and deepen future research from the device

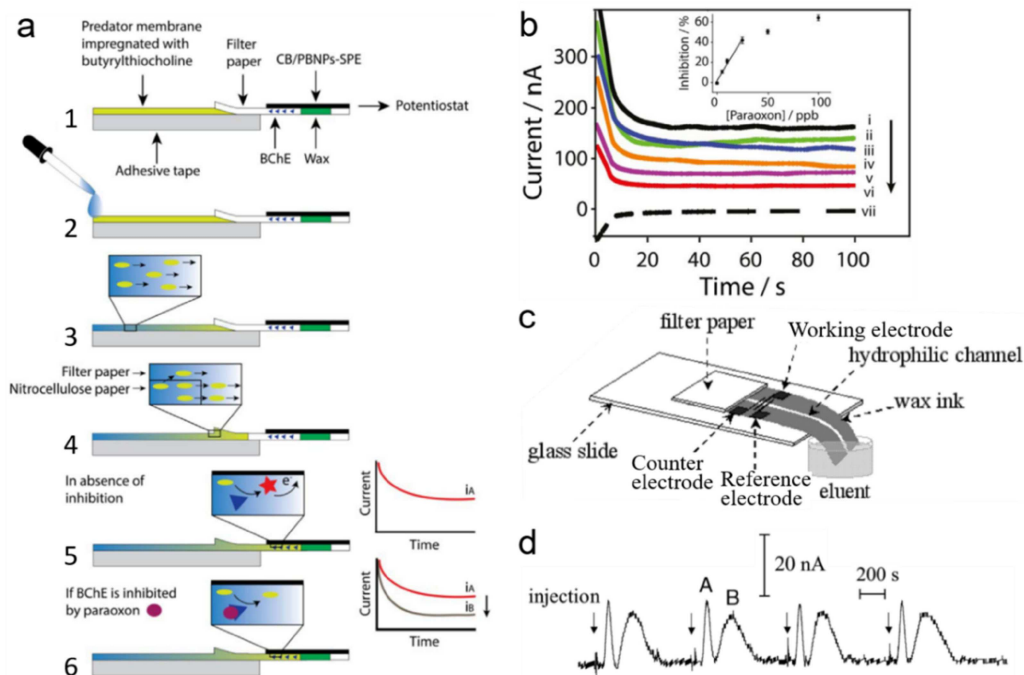


**Figure 9.** (a) Scheme of the working mechanism of the paper-based electrochemical biosensor for nerve agent detection. (b) Chronoamperometric curves obtained by analyzing paraoxon prepared in distilled water. Inset is the calibration plot. Reprinted with permission.<sup>[112]</sup> Copyright 2017 Elsevier. (c) Layout of the PDE-PED. (d) Chromatograms recorded at a PDE-PED for four replicate applications of samples containing ascorbic acid (peak A) and sunset yellow (peak B). Reprinted with permission.<sup>[111]</sup> Copyright 2013 Wiley-VCH.

itself and the analysis results, toward investigating the analysis process, including the analyte flow/permeation/dissolution behavior within the paper matrix and the electrochemical reaction taking place on the catalyst layer.

## 4. Energy Devices

Compared to those well-studied  $\mu$ PEDs for sensing applications, application of paper microfluidics in the energy sector is still at an infant stage. This emerging research topic is largely motivated by the growing demand for environmentally benign, miniaturized and disposable power supplies intended for single-use small electrochemical devices for sensing, display, diagnosis and/or therapy. To this end, paper-based microfluidic energy devices again demonstrate to be a promising option. Table 2 summarizes some recently developed paper-based microfluidic devices as power sources, together with their major components, fabrication methods, performance and features. As the key component of these devices, paper materials usually play a crucial role in determining the device performance,

which, however, are rarely being the focus of these investigations, despite the consensus that paper with higher wicking rate is usually preferred in constructing paper-based energy devices. Therefore, the information of paper type is also included in Table 2 for a fair comparison. In the following context, we will mainly focus on the recent advances in developing miniaturized battery and fuel cell devices following the paper-based microfluidic concept.

### 4.1. Batteries

In the early design of paper-based batteries, paper serves as electrode separator or reservoir to store redox reagents or to carry electrolyte. For instance, Ki Bang Lee developed a series of paper-based batteries composed of magnesium foil as anode, copper chloride impregnated filter paper as cathode and copper as current collector.<sup>[120–121]</sup> The batteries can be activated by wetting the paper with urine, saliva, or tap water, and deliver a maximum voltage of 1.56 V within 10 s after activation and a maximum power of 15.6 mW.<sup>[121]</sup> However, it can also be

**Table 2.** Summary of typical paper-based microfluidic energy devices.

Anode, fuel Cathode, oxidant	Fabrication method	Paper type (flow rate)	Electrolyte	$V_{\max}^{[a]}$ (V)	$P_{\max}^{[b]}$	Features	Ref.
Mg foil, Mg CuCl on paper, CuCl	Impregnating, laminating	Filter paper	Urine, saliva, tap water	1.56	15.6 mW	Biofluid activated battery	[114]
Al, AlCl <sub>3</sub> Ag, AgNO <sub>3</sub>	Stacking, com- pressing	Whatman Grade 1	Water	2.5 <sup>[c]</sup>	1.6 mW <sup>[c]</sup>	Integrated with a sensor, activated by analyte	[15]
Mg, MgCl <sub>2</sub> Ag, AgNO <sub>3</sub>	Wax-printing, or- igami	Whatman Grade 1 (4.3 mm/min)	Water	2.2	3.0 mW/ cm <sup>2</sup>	Integrated with a fluorescent assay	[115]
Carbon on paper, bacteria	Screen-printing, origami	Whatman Grade 1	Bacteria liquid	0.93 <sup>[c]</sup>	48 nW <sup>[c]</sup>	Bacteria-powered battery	[116]
Ni on paper, air Carbon, pBQ <sup>[d]</sup> Carbon, H <sub>2</sub> BQS <sup>[d]</sup>	Stacking	Ahlstrom	Anode: OA <sup>[d]</sup> cathode: KOH	0.75	6.8 mW/ cm <sup>2</sup>	Metal-free, capable to operate up to 100 min	[16]
Al foil Carbon paper, air	Cutting, stacking	Advantec filter paper	5 M NaOH	1.6	21 mW/ cm <sup>2</sup>	Paper channel reduces Al corrosion	[17]
Al foil Pd/C on graphite foil, air	Cutting, paint- ing, stacking	VWR417 (24 $\mu$ L/min)	1.5 M KOH	1.55	22.5 mW/ cm <sup>2</sup>	Long-time discharge without using gas diffusion electrode	[58]
PtRu/C on Au, CH <sub>3</sub> OH Pt/C on carbon pa- per, air	Cutting, laminat- ing	Whatman fusion 5 (80 $\mu$ L/min)	2 M KOH	0.55	4.4 mW/ cm <sup>2</sup>	The first paper-based microfluidic fuel cell	[19]
Graphite, HCOOH Graphite, air	Cutting, writing	Whatman	3.75 M H <sub>2</sub> SO <sub>4</sub>	0.33	32 mW/ cm <sup>2</sup>	Electrodes prepared by pencil stroking on paper	[117]
Pd/C on graphite foil, HCOOK Pd/C on graphite foil, air	Cutting, stacking	VWR417 (30 $\mu$ L/min)	1 M KOH	0.86	7.1 mW/ cm <sup>2</sup>	Stable power output up to 1 h	[37]
Glucose oxidase, glucose Laccase, air	Cutting, stacking	Whatman fusion 5 (30–20 $\mu$ L/min)	Phosphate buffer	0.6	45 $\mu$ W/ cm <sup>2</sup>	Enzymatic glucose/O <sub>2</sub> fuel cell operated in mild pH conditions	[118]
Ag nanowires, H <sub>2</sub> O <sub>2</sub> PB <sup>[d]</sup> on CNTs <sup>[d]</sup> , H <sub>2</sub> O <sub>2</sub>	Cutting, stacking	Whatman	1.5 M H <sub>2</sub> SO <sub>4</sub>	0.58	0.88 mW/ cm <sup>2</sup>	Single-stream cell using H <sub>2</sub> O <sub>2</sub> as both fuel and oxidant	[119]
Pt/C on carbon pa- per, H <sub>2</sub> Pt/C on carbon pa- per, air	Cutting, laminat- ing	Fusion 5, GE Health- care	KOH	1.0	25 mW	Paper-based hydrogen fuel cell cooperated with <i>in situ</i> H <sub>2</sub> generator	[18]

[a] Maximum voltage [b] Maximum power or maximum power density normalized to electrode area [c] 4 battery stack [d] pBQ: p-benzoquinone; H<sub>2</sub>BQS: hydroquinonesulfonic acid potassium salt; OA: oxalic acid; PB: Prussian Blue; CNTs: carbon nanotubes.

noticed that the power output decays over time, which might stem from the depletion of reactants at electrode surfaces, due to the non-fluidic configuration of the device. Anyhow, these paper-based batteries bring new ideas to fabricate low-cost and flexible power sources for miniaturized electronics, especially for those single-use ones.

Many of electrochemical sensors require external power supplies for sensing or displaying purposes, either using a battery or line voltage.<sup>[122]</sup> Ideal POC devices should be operated without appended equipment,<sup>[15]</sup> *i.e.*, self-powered devices integrated with power-generating units. Thom et al. reported the first self-powered  $\mu$ PAD, integrated with fluidic batteries and fluorescence assay for detecting  $\beta$ -D-galactosidase (a general marker for fecal contamination in water).<sup>[15]</sup> As shown in Figure 10a and b, the fluidic batteries present a stacked configuration, with the electrodes (Ag, Al), electrolyte (AgNO<sub>3</sub>, AlCl<sub>3</sub>) and salt bridge (NaNO<sub>3</sub>) preloaded into the specific paper layers in dry state. Figure 10c shows the cross section of the self-powered paper-based microfluidic fluorescent assay. When sample containing  $\beta$ -D-galactosidase is added into the device, it reacts with the preloaded 7-(D-galactosyloxy)coumarin in the assay region to form fluorescent dye 7-hydroxycoumarin.<sup>[123]</sup> Meanwhile, the sample wets the paper channel and triggers the primary batteries to power an on-board UV-LED, which enables the fluorescence readout of the 7-hydroxycoumarin (Figure 10d).<sup>[123]</sup> This work demonstrates for the first time the feasibility of integrating a miniaturized paper-based microfluidic battery into a sensing devices. Similarly, Zhang et al. reported a self-powered 3D origami microfluidic ECL biosensing device ( $\mu$ -s-OECLD), built with a primary battery (C | FeCl<sub>3</sub> | NaCl | AlCl<sub>3</sub> | Al), which can be directly activated by analyte solutions and provide a stable power output for 12 h. The  $\mu$ -s-OECLD can be used to detect glucose with luminol as ECL solution.<sup>[124]</sup> Koo et al. also presented an origami paper-based primary battery using magnesium as anode and silver as cathode.<sup>[115]</sup> A single battery is operated with 80  $\mu$ L of water, and produces an open circuit voltage (OCV) of 2.2 V and a power density of 3.0 mW/cm<sup>2</sup>. Two serial connected batteries are incorporated with a UV-LED for fluorescence detection of alkaline phosphatase.<sup>[115]</sup> Zhang et al. developed a flexible potential-tunable power system on paper. Owing to its origami configuration and the

addressable paper circuit switch, the paper-based energy device can be integrated with analytical platforms to prepare self-powered all-paper electronics.<sup>[125]</sup>

Bioenergy technologies have gained increasing research interests as green and renewable alternatives for energy conversion.<sup>[126]</sup> Among various bioenergy technologies, bacteria batteries, which can generate power from microbial metabolism, are promising technologies to provide green power.<sup>[127]</sup> Choi group proposed an origami paper-based bacteria battery, which can be connected in series by simply folding to meet various power needs (Figure 11a).<sup>[116]</sup> Upon adding one drop of bacteria-containing liquid derived from renewable and sustainable water or wastewater sources, the liquid flows through the microfluidic channels, reaches batteries and generates power (Figure 11b). An OCV of 0.93 V and a maximum output power of 48 nW (9.3  $\mu$ W/m<sup>2</sup>) can be obtained on a four-battery stack. Choi group further developed papertronic biobatteries with increased power output and longer shelf life, which were fabricated on conductive polymer coated filter paper, with exoelectrogenic bacterial as anode biocatalyst.<sup>[128]</sup> A simple drop of liquid (e.g., saliva) to the anode is sufficient to rehydrate the bacterial to generate electrons, thus activate the battery. An OCV of 2.9 V and a maximum output power of 45  $\mu$ W (1.4  $\mu$ W/cm<sup>2</sup>) can be achieved on a 16-battery stack, demonstrating good voltage and power scalability of these miniaturized batteries.

The disposal of large number of single-used electronics together with batteries (e.g., LIBs, other metal-containing primary batteries), and insufficient battery cycling infrastructure cause severe environmental issues. Paper-based microfluidic batteries discussed above are great examples as disposable energy sources due to their biocompatible nature. However, the power output of these batteries is still at microwatt-level, which limits their usage in some electronics with higher power consumption. Esquivel et al. developed a biotically metal-free single-use battery PowerPAD.<sup>[16]</sup> The PowerPAD, which can provide mW-level power, is made of cellulose, carbon paper, beeswax and organic redox species (Figure 11c). A pair of commercially available quinone compounds, p-benzoquinone and hydroquinonesulfonic acid potassium salt, were chosen as redox species.<sup>[129]</sup> As shown in Figure 11d, the battery is

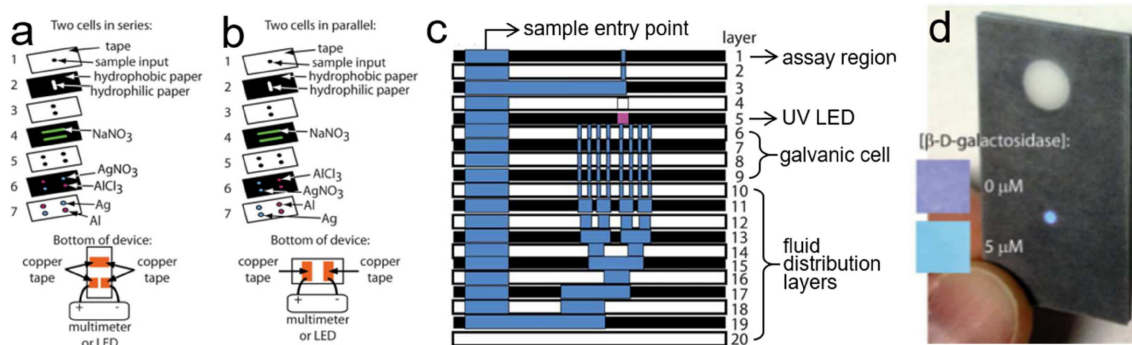


**Figure 10.** Self-powered paper-based microfluidic devices using fluidic batteries connected in (a) series or (b) parallel. (c) Cross section of the self-powered paper-based microfluidic fluorescent assay. (d) "Colorimetric" output provided by the on-chip fluorescence assay as a function of the concentration of  $\beta$ -D-galactosidase in the sample. Reprinted with permission.<sup>[15]</sup> Copyright 2012 Royal Society of Chemistry.

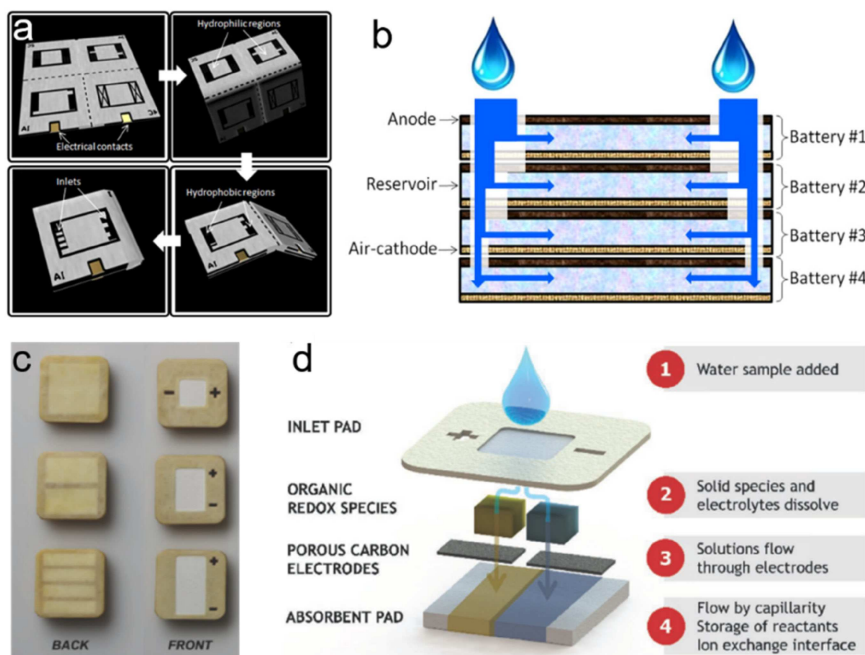


**Figure 11.** (a) Schematic diagrams of the 3D origami bacteria battery showing the folding steps. (b) Schematic diagram of the cross section of the bacteria battery stack. Reprinted with permission.<sup>[116]</sup> Copyright 2015 Elsevier. (c) Image of the PowerPAD: single cell (up), 2-cell stack (middle), and 4-cell stack (bottom). (d) Schematic diagram and working principle of the PowerPAD. Reprinted with permission.<sup>[16]</sup> Creative Commons license 4.0 (CC BY-NC 4.0)

designed as a vertical capillary flow cell, composed of several patterned cellulose layers stacked together. The battery can be activated by adding water to the top inlet pad. When water flows to each half cell and dissolves the redox species and electrolytes, the dissolved reactant species flow through the carbon electrodes toward the absorbent pad. The battery starts generate power once the anolyte and catholyte contact with each other in the absorbent pad. The co-laminar flow in the paper matrix enables the battery operate for up to 100 min. An OCV of 0.75 V and maximum power density of 6.8 mW/cm<sup>2</sup> can be achieved on a single battery. However, using the toxic quinone compounds as the redox species raises the doubt of the environment friendly disposability of these batteries.

Portable and disposable electronic devices usually need power sources that are not only miniaturized in size, but also possessing high energy and power density. Metal-oxygen redox reactions generate high energy density because of their high redox potentials and the abundant valance electrons in metal that take part in the redox process.<sup>[130–131]</sup> Therefore, metal-air batteries hold great promise in powering those portable devices. Among various metal-air batteries, Al-air battery is an attractive candidate because of the high abundance, low price and environmentally benign nature of aluminum.<sup>[132–133]</sup> However, several scientific and technical issues of Al-air batteries, such as self-discharge, anode passivation and the use of expensive air electrode, have greatly hindered their broad-based applications.<sup>[130,134–136]</sup>

Shen et al. implemented the paper microfluidic concept to construct an innovative paper-based microfluidic Al-air battery ( $\mu$ Al-air). The aforementioned issues faced by conventional Al-air batteries can be largely relieved or even eliminated on the

$\mu$ Al-air battery. As shown in Figure 12a and b, the microfluidic paper channel is sandwiched between an Al foil (anode) and a piece of catalyst coated graphite foil (cathode) without using any costly air electrode. The Al anode is separated from the electrolyte before use, which can eliminate the self-discharge and prolong the shelf life. The paper-based  $\mu$ Al-air battery can be activated by wetting the paper channel using electrolyte. An absorbent pad is placed at the end of the paper channel to maintain a steady flow rate (24  $\mu$ L/min) of electrolyte. The discharge measurements (Figure 12c) show that the  $\mu$ Al-air battery presents impressive specific capacity (2750 Ah/kg) and energy density (2900 Wh/kg), which are much superior to Al-air battery without microfluidic configuration. The superior performance is largely benefit from the microfluidic configuration, which can take effect by preventing the accumulation of the discharge product as reflected by the complete consumption of Al foil (Figure 12c), and more importantly enabling the continuous mass transfer of oxygen to the cathode catalyst layer (Figure 12d). The  $\mu$ Al-air battery can also be activated using neutral electrolyte (NaCl solution), which gives a capacity of 2200 Wh/kg, shedding a new light on developing future sustainable energy storage/conversion devices. Wang et al. also developed a low-cost paper-based Al-air battery for miniwatt-level applications.<sup>[117,137]</sup> An OCV of 1.6 V, a peak power density of 21 mW/cm<sup>2</sup> and a specific capacity of 1273 Ah/kg were obtained. Compared with Al-air battery fabricating on conventional microfluidic channel, the Al-air battery on paper microfluidic channel exhibits much higher capacity. The superior performance is speculated to benefit from the porous and tortuous microstructure of paper, which impedes the diffusive transport of OH<sup>-</sup>, and consequently suppresses Al corrosion.

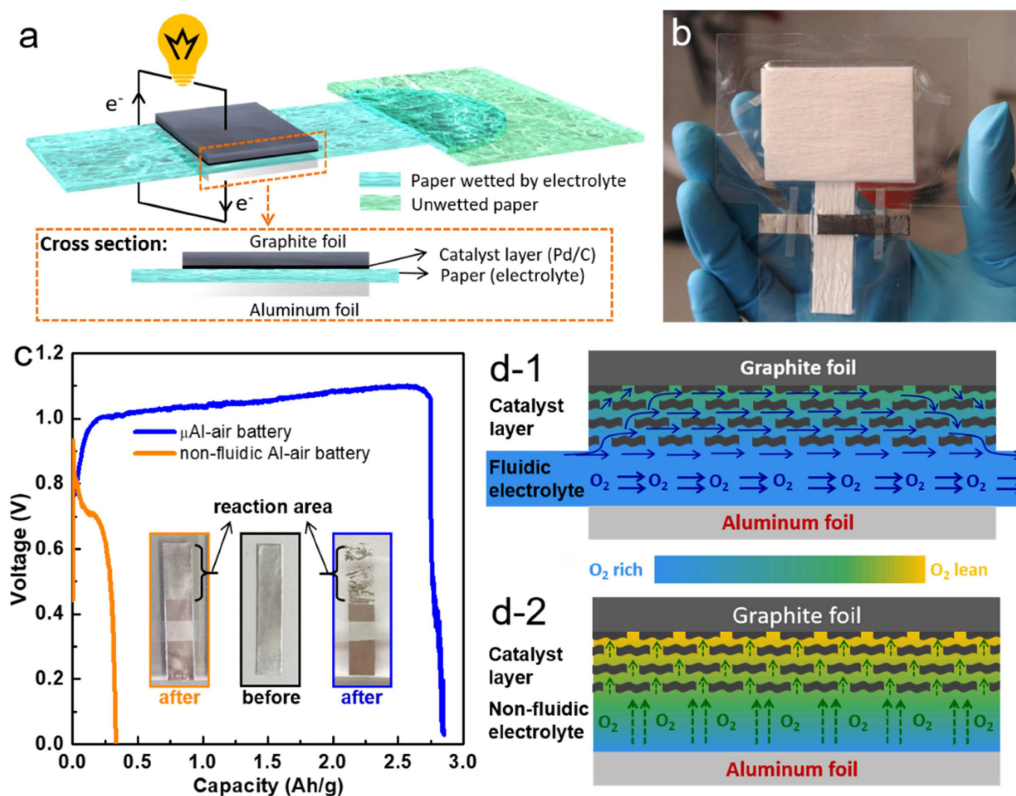


**Figure 12.** (a) Scheme of a paper-based  $\mu$ Al-air battery. (b) A paper-based  $\mu$ Al-air pouch battery from top view. (c) Discharge curves of fluidic and non-fluidic Al-air battery. The insets in (c) are the optical images of the anode aluminum foils before and after discharge. (d) Schematic illustrations of cross-sectional  $O_2$ -rich/lean electrolyte distribution in (d-1) fluidic and (d-2) non-fluidic Al-air battery. Reprinted with permission.<sup>[58]</sup> Creative Commons license 3.0 (CC BY-NC 3.0).

## 4.2. Fuel Cells

Fuel cell is an environmentally friendly energy conversion system with high energy density, high efficiency and good reliability.<sup>[38]</sup> In a conventional polymer electrolyte membrane fuel cell, the energy source (fuel and oxidant) and energy converter (fuel cell devices) are separated, thus a mass transfer of the energy source to the electrodes has to be carefully manipulated. A proton exchange membrane is always needed to separate the two half-cells and to transfer proton from the anode to cathode. The slow kinetics of cathodic oxygen reduction reaction (ORR) represents a major obstacle limiting fuel cell performance.<sup>[138–141]</sup> Even though ORR has a faster kinetics in alkaline than in acidic electrolyte, it remains a non-trivial task to develop reliable anion exchange membranes for alkaline fuel cells.<sup>[142–144]</sup> Whitesides et al. proposed the first membraneless microfluidic fuel cell concept in 2002. In their work, the anolyte and catholyte flow parallel to each other in one microfluidic channel without membrane separation, and only diffusive mixing occurs across the interface between these two streams. An OCV of 1.52 V is obtained at a flow rate of 25  $\mu$ L/s based on vanadium redox couple.<sup>[145]</sup> Since then, the membraneless microfluidic fuel cells have been demonstrated by using different electrode catalysts, as well as different fuels and oxidants in both acid and alkaline solutions.<sup>[146–157]</sup> However, the main issue that limits the real application of membraneless microfluidic fuel cell again lies in the use of external pumping

devices, which adds to system cost and makes it challenging to miniaturize the device for portable applications. A solution was proposed by Esquivel et al. in 2014 by presenting the first paper-based self-pumping microfluidic fuel cell.<sup>[19]</sup> As we have discussed in Section 2.2, fluids driven by capillary action within a paper matrix are at low Reynold's number, i.e., laminar flow. Paper-based fuel cells benefit from the two parallel laminar flows on paper, enabling efficient separation of anolyte and catholyte without using any ionic exchange membrane or external pump, as shown in Figure 3a.

In the paper-based microfluidic fuel cell proposed by Esquivel et al. (Figure 13a), the anode is placed under the paper strip, while the cathode is attached on top to facilitate oxygen access from the atmosphere. The fuel cell operates on the simultaneous addition of anolyte (methanol and KOH) and catholyte (KOH) in each inlet sample pads. An OCV of 0.55 V and a maximum power density of 4.4  $mW/cm^2$  can be achieved on the paper-based microfluidic fuel cell. The fuel cell is able to provide a continuous power more than 2.0  $mW/cm^2$  for 4.2 min when fed with 150  $\mu$ L reactant (Figure 13c). The configuration of the fuel cell was improved toward real application in which the lateral flow test is wetted with a single fluid, as shown in Figure 13b. Electrolyte (KOH) and fuel (methanol) are stored in Fusion 5 membrane and agar gel respectively. Within this design, the fuel cell is able to be activated by feeding small amount of water to the inlet pads. The fuel cell is able to output power at 1.75  $mW/cm^2$  for 4.5 min by using the single inlet

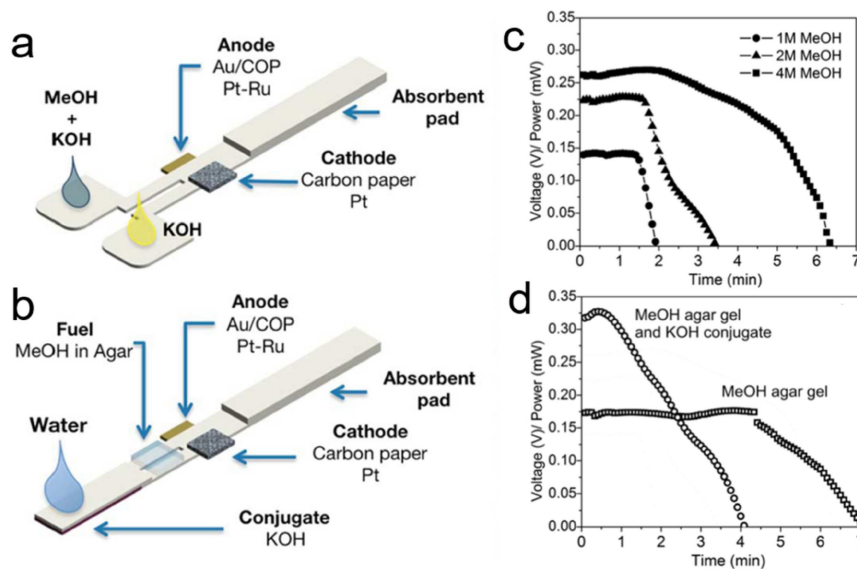


**Figure 13.** (a) Schematic presentation of a paper-based microfluidic fuel cell. (b) Concept of a single fluidic lateral flow test strip fuel cell activated with water. (c) Power output of a paper-based microfluidic fuel cell based on bi-laminar flow at a current load of 1 mA. (d) Power output of a paper-based microfluidic fuel cell based on laminar flow at a current load of 1 mA. Reprinted with permission,<sup>[19]</sup> Creative Commons license 3.0.

design (Figure 13d). The power yield by the lateral flow-based fuel cells meet the power needs of many POC devices, e.g., pregnancy tests and glucometers, and the unique electrochemical features and the design of the fuel cells make them capable to generate power by directly using the analyte solution.

Various investigations have been done to explore other possibilities of paper-based microfluidic fuel cell. Arun et al. reported a paper-based membraneless formic acid fuel cell operated in self-pumping and air-breathing mode by incorporating HB-pencil stroked graphite as both anode and cathode electrodes (Figure 14a).<sup>[117]</sup> This simple fuel cell generates a constant OCV of 0.27 V for up to 1000 min, and a maximum power density of 32 mW/cm<sup>2</sup>. This pencil-on-paper technique brings novel ideas to fabricate simple and low-cost paper-based microfluidic fuel cells. Copenhagen et al. presented the first paper-based microfluidic direct formate fuel cell (DFFC) that uses formate and hydrogen peroxide as the anode fuel and cathode oxidant, respectively.<sup>[158]</sup> As shown in Figure 14b, a Y-shaped paper channel is designed for the co-laminar flow of anolyte and catholyte. The dots on the paper channel are Pd/C (anode catalyst) and colloidal graphite (cathode catalyst), with brass plates as current collectors. A maximum power density of 2.5 mW/mg<sub>Pd</sub><sup>-1</sup> (0.5 mW/cm<sup>2</sup>) can be achieved on the fuel cell. The performance of the paper-based microfluidic DFFC was further improved by Galvan and co-workers.<sup>[159]</sup> In their design (Figure 14c), current collectors (steel mesh) are bonded to the Y shaped paper channel using silver epoxy, and the catalysts (1.5 mg/cm<sup>2</sup> Pd/C for anode, carbon for cathode) are painted directly onto the silver epoxy attached steel mesh. An increased maximum power density of 2.53 mW/cm<sup>2</sup> and OCV of 1.1 V can be obtained on this design. Despite the blooming of research of paper-based microfluidic fuel cells, the influence of paper

materials, which serves as a key structural component, however, remains elusive for a long time.

Various limiting structural parameters of paper-based microfluidic fuel cells including textural properties of paper materials, were identified and debottlenecked by Shen et al.<sup>[37]</sup> In their design (Figure 14d), both the anode and cathode electrodes are prepared by coating ultra-low amount of Pd/C catalyst on commercial graphite foil, and then placed on the Y-shaped paper channel. The influence of fuel crossover, cell resistance, limitations at cathode/anode, and especially the properties of the microfluidic paper channel have been systematically investigated. Among various parameters, for the first time it is unraveled that the overall performance of a paper-based microfluidic fuel cell is largely dependent on the textural properties of the paper channels (Figure 14e and f). It discloses that a greater flow rate which is achieved on paper channel with larger pore size would result in higher OCV and peak power density. The performance enhancement stems from the minimized fuel/oxidant depletion at the electrodes and suppressed fuel crossover. Technically, an OCV of 0.86 V and a maximum power density of 7.10 mW/cm<sup>2</sup> can be achieved on a single cell, and the maximum power output can be maintained for at least 1 h. These results indicate that controlling the microfluidic behavior on paper by choosing paper with various textural properties is of great importance for constructing paper-based microfluidic electronics.

Compared with conventional fuel cells that use precious metal as catalysts, the enzymatic biofuel cells utilize enzymes to oxidize the fuel (e.g., sugar, alcohols), holding potential as a relatively inexpensive power source for bionic implants.<sup>[160–161]</sup> Gonzalez-Guerrero et al. presented an enzymatic paper-based microfluidic fuel cell, with the anode being modified with redox polymer linked to glucose oxidase where glucose is oxidized, and the cathode containing mixture of laccase enzyme and

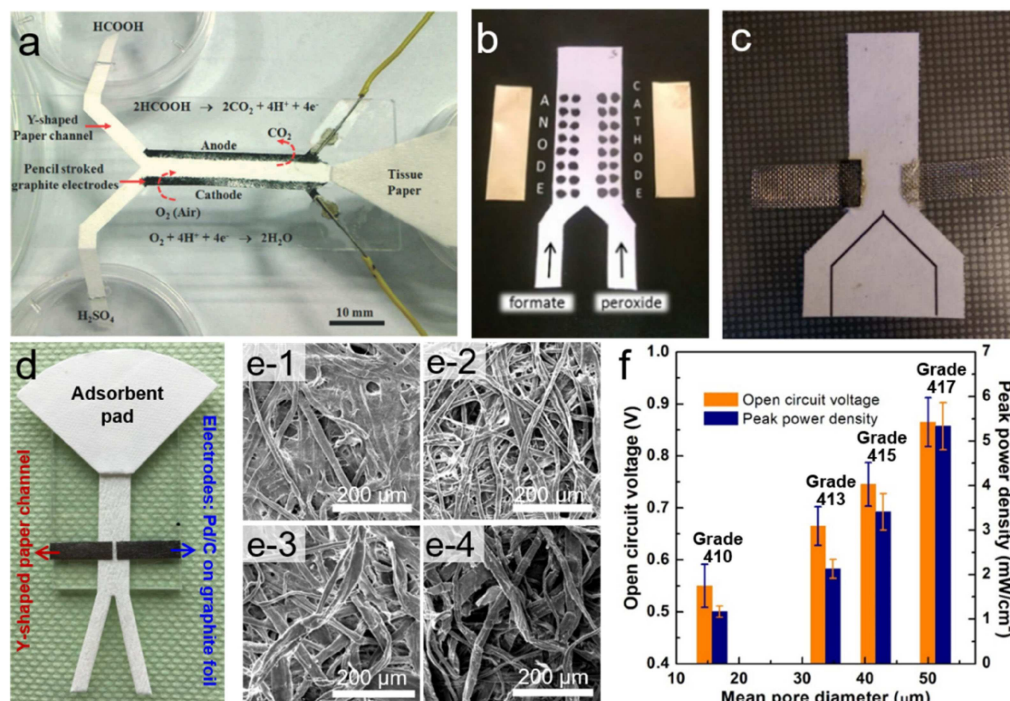


**Figure 14.** (a) A self-pumping fuel cell consisting of a paper channel and pencil stroked electrodes. Reprinted with permission.<sup>[117]</sup> Copyright 2014 Royal Society of Chemistry. (b) Paper-based microfluidic DFFC with catalyst painted on the paper channel. Reprinted with permission.<sup>[158]</sup> Copyright 2015 Wiley-VCH. (c) Paper-based microfluidic DFFC using painted anode electrode bonded with steel mesh. Reprinted with permission.<sup>[159]</sup> Copyright 2016 Wiley-VCH. (d) Paper-based microfluidic fuel cell with Y-shaped paper channel, Pd/C coated graphite electrodes and a fan-shaped adsorbent pad. (e) SEM images of different paper channels: Grade 410 (e-1), Grade 413 (e-2), Grade 415 (e-3), Grade 417 (e-4). (f) Comparisons of OCV and peak power density of paper-based microfluidic fuel cells fabricated with different papers. Reprinted with permission.<sup>[37]</sup> Copyright 2019 Elsevier.

anthracene-modified multi-wall carbon nanotubes to catalyze ORR.<sup>[118]</sup> When the biofuel cell is operated in a Y-shaped paper channel (Figure 15a), an OCV of 0.6 V and a maximum power density of 45  $\mu\text{W}/\text{cm}^2$  can be obtained (Figure 15c). In order to achieve an easy use for real application, the cell configuration is improved by replacing the Y-shaped channel with an I-shaped channel (Figure 15b), on which the cell is activated by adding a single electrolyte. Although the efficiency of the system decreased compared with the Y-shaped cell (Figure 15c), the single-stream configuration is easier to be implemented in a real application, e.g., a lateral flow test strip. Narvaez Villarrubia et al. reported an enzymatic fuel cell with single-stream design that employed an anode based on glucose dehydrogenase, a cathode based on bilirubin oxidase and a paper microfluidic channel.<sup>[162]</sup> The paper channel consists of a rectangular section appended to a fan-shaped section, which is proved to be a steady microfluidic transport media and guarantees the continuous supply of glucose to the anode.<sup>[56]</sup> Thus, a power output of 0.4 mW can be maintained for 16 days. Moreover, commercial beverage can be used as fuel to operate the cell. Yan et al. also developed a single-stream paper-based microfluidic fuel cell by using  $\text{H}_2\text{O}_2$  as both fuel and oxidant.<sup>[119]</sup> The dual role of  $\text{H}_2\text{O}_2$  is realized by selecting silver nanowires and carbon nanotube-supported PB as oxidation and reduction catalysts, respectively. The fuel cell is simply fabricated by placing the two electrodes symmetrically on a rectangular paper strip. An

OCV of 0.58 V and peak power density of 0.88  $\text{mW}/\text{cm}^2$  can be achieved on the cell, respectively.

Hydrogen fuel cell is the most widely studied fuel cell system due to its high energy density and zero-emission of carbon dioxide. However, one major challenge to develop portable hydrogen fuel cell is the storage and release of  $\text{H}_2$ . Esquivel et al. proposed a solution toward this challenge by integrating a paper-based hydrogen fuel cell with a customized chemical heater that produces hydrogen *in situ* upon the addition of a liquid.<sup>[18]</sup> As shown in Figure 15d, after adding liquid to the inlet, part of the liquid flows into the bottom paper channel and dissolve the stored NaCl, triggering the reaction of magnesium and water to produce  $\text{H}_2$ , while other liquid travels through the upper paper channel and dissolved the stored KOH, then driving KOH electrolyte to the fuel cell electrodes. The continuously generated  $\text{H}_2$  is oxidized at the bottom electrodes, while the  $\text{O}_2$  from air is reduced at the top electrode. Figure 15e shows the picture of the final device, which exhibits a compact configuration. The time-lapse performance of the paper-based fuel cell (Figure 15f) shows that it is able to provide a power around 25 mW for more than 6 min and then decreases steadily until it ceased to function after 60 min. The maximum output power density delivered by this device yields 4.8  $\text{mW}/\text{cm}^2$  (normalized to the total device footprint), which is comparable to the power if coin cell batteries (8.7  $\text{mW}/\text{cm}^2$ ) currently used in disposable portable devices.

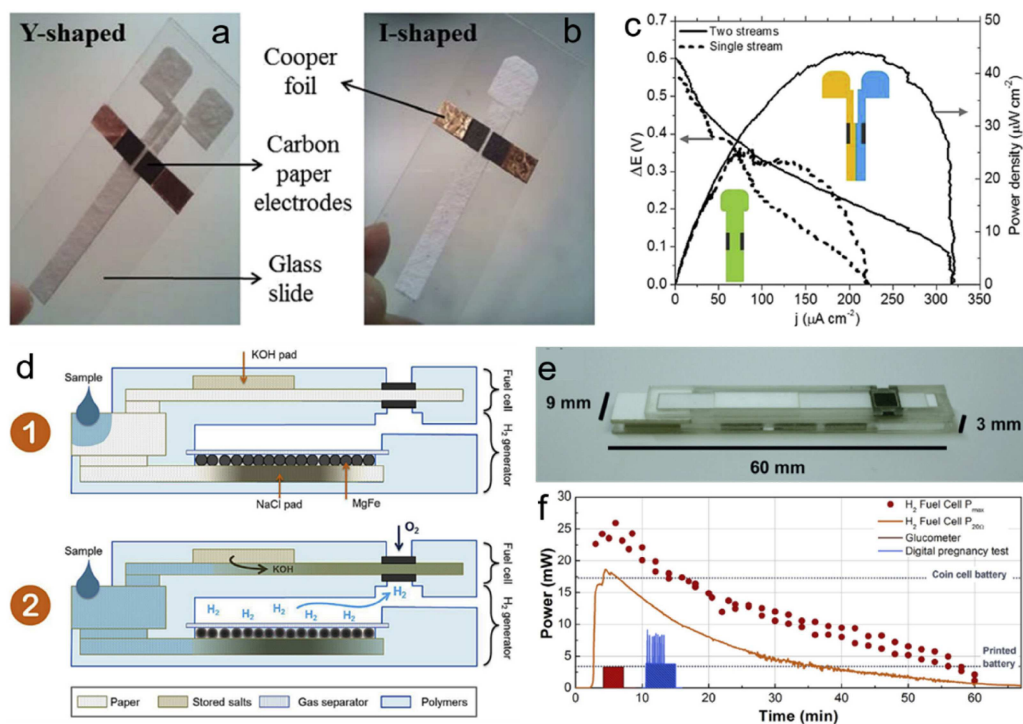


**Figure 15.** Paper-based enzymatic fuel cells fabricated on (a) Y-shaped and (b) I-shaped paper channels. (c) Polarization curves of paper-based enzymatic fuel cells. Reprinted with permission.<sup>[118]</sup> Copyright 2016 Wiley-VCH. (d) Cross section diagram of paper-based hydrogen fuel cell. (e) Isometric view of the device with dimensions. (f) Performance of the paper-based fuel cell. Reprinted with permission.<sup>[18]</sup> Copyright 2017 Elsevier.

Paper materials have already been employed as a key component in fabricating low-cost, eco-friendly portable and flexible power sources. In the early design of paper-based power sources, paper is mainly employed as electrode separator, electrolyte/redox species reservoir, or electrode, and concentrations are mainly focused on how to assemble a battery/cell operable at low-cost. With the development of paper microfluidics, researchers realize that paper can be employed as microfluidic channel to continuously and spontaneously transport electrolyte (reactant) solution with steady flow rate in a laminar way, which enables the battery to discharge for long time with a stable output power. Moreover, the co-laminar flow on paper makes it possible to fabricate more sophisticated power sources, such as fuel cells, and more efforts are spent to investigate how the configuration/composition (e.g., paper properties, microfluidic behavior, electrode catalysts, redox species) of paper-based power source influence their electrochemical performance.

## 5. Summary and Outlook

The advances reviewed here demonstrate that cellulose paper or paper-based materials provide great opportunities to design and fabricate low-cost, green, portable, user-friendly microfluidic electronics in the field of medical diagnosis, environment monitoring, and energy storage/conversion. The abundance of natural cellulose and the advanced paper manufacturing technique make paper one of the most widely used and

cheapest substrate all around the world. The fibrous and porous nature of paper enable it to act as microfluidic carrier and eliminate the use of external pressure control system (e.g., pumps), making it possible to miniaturize the size and reduce the whole cost of the microfluidic electrochemical devices. The microfluidic behavior on paper, e.g., fluid pattern and flow rate, can be predicted and designed by selecting proper paper type, constructing microfluidic channel with various paper geometry (e.g., multi-channel paper substrate and 3D paper-based microfluidic stack), or paper functionalization based on the well-defined theory. Ever since 2009, paper-based electrochemical devices have been widely studied in the field of POC diagnosis and environment sensing. The catalyst preparation, electrode assembling, and device configuration have been intensively investigated toward better analytical/sensing performance. Multiplexed 2D/3D designs based on paper-based microfluidics provide an efficient platform where sample preparation, analyte separation and transfer, active reagent storage and release, as well as multi-detection can be proceed in a facile manner. Besides diagnosis and sensing, paper-based microfluidics also provides new ideas and methods to fabricate miniaturized power supply systems for portable applications. Some batteries and sensing systems can be integrated together on paper to construct self-powering sensor, in which the flow of analyte can activate the battery to generate power for the sensing process. Paper-based flexible and self-powering sensors show great potential to become part of the core of the IoT revolution, which demands system's mobility and self-powering functionality. For fuel cells, the co-laminar flow of anolyte and catholyte

can be achieved on the paper without using expensive proton/hydroxyl ion exchange membrane. Many efforts have been done to improve the configuration of the paper-based microfluidic fuel cell for easy operation and high performance. For example, some fuel cells are able to run by single flow rather than multi-flow, and hydrogen fuel cell can also be realized on paper by overcoming the hydrogen storage issues. The paper-based microfluidic batteries and fuel cells are versatile in the redox species, such as glucose-oxygen, bacteria-air, metal-air, hydrogen-oxygen et al., making them possible to meet various power requirements. Thus the research results from the bio-enzyme, electro-catalyst, air electrode, and electrolyte can be transferred to fabricate highly performance paper-based microfluidic batteries and fuel cells.

The development of paper-based microfluidic electronics is targeting the real commercialized applications in the near future. However, many researches still remain in the proof-of-concept level. For paper-based electrochemical microfluidic sensors, even though paper is an inexpensive and eco-friendly material, the electrode material or modifier might be costly and toxic. Moreover, sample preparation such as dilution and pH controlling is usually required in the sensing process, which are complex for users without expertise. The analysis processes are operated with a potentiostat, which are not commonly available, and the interpretation of the output data is unfamiliar to general people. Thus the electrochemical sensing system should integrate the sample preparation, electrodes for sensing, power source, electrochemical method and understandable data reader. An easy way to reach this goal is to use commercially available glucometer, or develop potentiostat for home-use. For the paper-based microfluidic batteries and fuel cells, strong acid or alkaline electrolyte should be avoided in concern of safety reasons. The ideal protocol is to store the redox species and electrolyte inside the device and activate the battery/cell by directly adding water or neutral solution available in daily life, such as NaCl solution. Other limitations come from the catalysts and electrodes, especially for the cathode part. For example, expensive platinum-based catalysts and gas diffusion electrode are needed to accelerate the ORR kinetics and the mass transfer of oxygen from air to the catalyst layer. Besides, some redox species are toxic, and thus these paper-based microfluidic batteries or fuel cells are not really disposable. Last but not least, microfluidics within paper largely depends on the paper properties and configuration. However, the selection criteria of paper substrate are not always clearly discussed in the design of paper-based microfluidic devices.

Even though the paper-based microfluidic electronics still face various problems to be become commercialized, the fast development of science and technology makes us believe that it is only a matter of time to solve these aforementioned issues. For example, many research groups are working on developing inexpensive and environmentally friendly electrode materials or catalysts toward electrochemical analysis and power generation. Some researchers are investigating the influence of the paper properties and microfluidic behavior on the electrochemical device performance. In the future, 3D printing, electro-spinning techniques may play an important role in manufactur-

ing paper-based microfluidic electronics in large scale, and computational techniques may facilitate the development of paper-based microfluidic electronics by simulating the microfluidic behavior and predicting its effect on the device performance. In summary, we are heading toward a new generation of microfluidic electronics base on paper. Along with the continuous deepening of research, the paper-based microfluidic electrochemical devices will finally be employed in practical applications, and bring convenience and benefit to people's lives.

## Acknowledgements

The authors acknowledge the funding from the European Research Council under the European Union's Horizon 2020 research and innovation program (No. 681719) and the funding by the Deutsche Forschungsgemeinschaft (DFG, German Research Foundation) within the project ET-101/15-1. L.-L.S. acknowledges the financial support of the China Scholarship Council (No. 201506210077).

## Conflict of Interest

The authors declare no conflict of interest.

**Keywords:** batteries · electrochemical sensors · fuel cells · microfluidics · paper devices

- [1] S. C. Terry, J. H. Jerman, J. B. Angell, *IEEE Trans. Electron Devices* **1979**, *26*, 1880–1886.
- [2] G. M. Whitesides, *Nature* **2006**, *442*, 368–373.
- [3] D. Erickson, D. Li, *Anal. Chim. Acta* **2004**, *507*, 11–26.
- [4] S. Haerberle, R. Zengerle, *Lab Chip* **2007**, *7*, 1094–1110.
- [5] M. Safdar, J. Jänis, S. Sanchez, *Lab Chip* **2016**, *16*, 2754–2758.
- [6] E. K. Sackmann, A. L. Fulton, D. J. Beebe, *Nature* **2014**, *507*, 181.
- [7] N.-T. Nguyen, S. T. Wereley, S. A. M. Shaegh, *Fundamentals and applications of microfluidics*, Artech house, **2019**.
- [8] C.-C. Wang, J. W. Hennek, A. Ainla, A. A. Kumar, W.-J. Lan, J. Im, B. S. Smith, M. Zhao, G. M. Whitesides, *Anal. Chem.* **2016**, *88*, 6326–6333.
- [9] W. Dungchai, O. Chailapakul, C. S. Henry, *Anal. Chem.* **2009**, *81*, 5821–5826.
- [10] H. Liu, Y. Xiang, Y. Lu, R. M. Crooks, *Angew. Chem. Int. Ed.* **2012**, *51*, 6925–6928; *Angew. Chem.* **2012**, *124*, 7031–7034.
- [11] N. Dossi, R. Toniolo, A. Pizzariello, F. Impellizzieri, E. Piccin, G. Bontempelli, *Electrophoresis* **2013**, *34*, 2085–2091.
- [12] S. Cinti, C. Minotti, D. Moscone, G. Palleschi, F. Arduini, *Biosens. Bioelectron.* **2017**, *93*, 46–51.
- [13] M. Medina-Sánchez, M. Cadevall, J. Ros, A. Merkoçi, *Anal. Bioanal. Chem.* **2015**, *407*, 8445–8449.
- [14] L.-L. Shen, G.-R. Zhang, W. Li, M. Biesalski, B. J. Eitzold, *ACS Omega* **2017**, *2*, 4593–4603.
- [15] N. K. Thom, K. Yeung, M. B. Pillion, S. T. Phillips, *Lab Chip* **2012**, *12*, 1768–1770.
- [16] J. P. Esquivel, P. Alday, O. A. Ibrahim, B. Fernández, E. Kjeang, N. Sabaté, *Adv. Energy Mater.* **2017**, *7*, 1700275.
- [17] Y. Wang, H. Y. Kwok, W. Pan, H. Zhang, X. Lu, D. Y. Leung, *Appl. Energy* **2019**, *251*, 113342.
- [18] J. Esquivel, J. Buser, C. Lim, C. Domínguez, S. Rojas, P. Yager, N. Sabaté, *J. Power Sources* **2017**, *342*, 442–451.
- [19] J. Esquivel, F. Del Campo, J. G. de la Fuente, S. Rojas, N. Sabate, *Energy Environ. Sci.* **2014**, *7*, 1744–1749.

- [20] A. W. Martinez, S. T. Phillips, M. J. Butte, G. M. Whitesides, *Angew. Chem. Int. Ed.* **2007**, *46*, 1318–1320; *Angew. Chem.* **2007**, *119*, 1340–1342.
- [21] Y. Zhang, L. Zhang, K. Cui, S. Ge, X. Cheng, M. Yan, J. Yu, H. Liu, *Adv. Mater.* **2018**, *30*, 1801588.
- [22] B. Yao, J. Zhang, T. Kou, Y. Song, T. Liu, Y. Li, *Adv. Sci.* **2017**, *4*, 1700107.
- [23] J. L. Osborn, B. Lutz, E. Fu, P. Kauffman, D. Y. Stevens, P. Yager, *Lab Chip* **2010**, *10*, 2659–2665.
- [24] N. Blow, *Nat. Methods* **2009**, *6*, 683.
- [25] A. W. Martinez, S. T. Phillips, E. Carrilho, S. W. Thomas III, H. Sindi, G. M. Whitesides, *Anal. Chem.* **2008**, *80*, 3699–3707.
- [26] A. W. Martinez, S. T. Phillips, G. M. Whitesides, *PNAS* **2008**, *105*, 19606–19611.
- [27] A. K. Ellerbee, S. T. Phillips, A. C. Siegel, K. A. Mirica, A. W. Martinez, P. Striehl, N. Jain, M. Prentiss, G. M. Whitesides, *Anal. Chem.* **2009**, *81*, 8447–8452.
- [28] Y. Lu, W. Shi, L. Jiang, J. Qin, B. Lin, *Electrophoresis* **2009**, *30*, 1497–1500.
- [29] Y. Lu, W. Shi, J. Qin, B. Lin, *Anal. Chem.* **2009**, *82*, 329–335.
- [30] A. W. Martinez, S. T. Phillips, Z. Nie, C.-M. Cheng, E. Carrilho, B. J. Wiley, G. M. Whitesides, *Lab Chip* **2010**, *10*, 2499–2504.
- [31] J. Mettakoonpitak, K. Boehle, S. Nantaphol, P. Teengam, J. A. Adkins, M. Srisa-Art, C. S. Henry, *Electroanalysis* **2016**, *28*, 1420–1436.
- [32] K. Yamada, H. Shibata, K. Suzuki, D. Citterio, *Lab Chip* **2017**, *17*, 1206–1249.
- [33] A. Pal, H. E. Cuellar, R. Kuang, H. F. Caurin, D. Goswami, R. V. Martinez, *Adv. Mater. Technol.* **2017**, *2*, 1700130.
- [34] C. Zhao, M. M. Thuo, X. Liu, *Sci. Technol. Adv. Mater.* **2013**, *14*, 054402.
- [35] Z.-X. Zou, J. Wang, H. Wang, Y.-Q. Li, Y. Lin, *Talanta* **2012**, *94*, 58–64.
- [36] P. B. Lillehoj, M.-C. Huang, N. Truong, C.-M. Ho, *Lab Chip* **2013**, *13*, 2950–2955.
- [37] L.-L. Shen, G.-R. Zhang, T. Venter, M. Biesalski, B. J. Etzold, *Electrochim. Acta* **2019**, *298*, 389–399.
- [38] C. K. Dyer, *J. Power Sources* **2002**, *106*, 31–34.
- [39] A. Avoundjian, V. Galvan, F. A. Gomez, *Micromachines* **2017**, *8*, 222.
- [40] D. M. Cate, J. A. Adkins, J. Mettakoonpitak, C. S. Henry, *Anal. Chem.* **2014**, *87*, 19–41.
- [41] C. Carrell, A. Kava, M. Nguyen, R. Menger, Z. Munshi, Z. Call, M. Nussbaum, C. Henry, *Microelectron. Eng.* **2019**, *206*, 45–54.
- [42] W. J. Paschoalino, S. Kogikoski Jr, J. T. Barragan, J. F. Giarola, L. Cantelli, T. M. Rabelo, T. M. Pessanha, L. T. Kubota, *ChemElectroChem* **2019**, *6*, 10–30.
- [43] J. Hu, S. Wang, L. Wang, F. Li, B. Pingguan-Murphy, T. J. Lu, F. Xu, *Biosens. Bioelectron.* **2014**, *54*, 585–597.
- [44] N. A. Meredith, C. Quinn, D. M. Cate, T. H. Reilly, J. Volckens, C. S. Henry, *Analyst* **2016**, *141*, 1874–1887.
- [45] M. M. Gong, D. Sinton, *Chem. Rev.* **2017**, *117*, 8447–8480.
- [46] K. Yamada, H. Shibata, K. Suzuki, D. Citterio, *Lab Chip* **2017**, *17*, 1206–1249.
- [47] D. Tobjörk, R. Österbacka, *Adv. Mater.* **2011**, *23*, 1935–1961.
- [48] H. Zhu, Z. Fang, C. Preston, Y. Li, L. Hu, *Energy Environ. Sci.* **2014**, *7*, 269–287.
- [49] N. Lavoine, I. Desloges, A. Dufresne, J. Bras, *Carbohydr. Polym.* **2012**, *90*, 735–764.
- [50] S. Li, C. Zhang, S. Wang, Q. Liu, H. Feng, X. Ma, J. Guo, *Analyst* **2018**, *143*, 4230–4246.
- [51] M. Safdar, J. Janis, S. Sanchez, *Lab Chip* **2016**, *16*, 2754–2758.
- [52] R. F. Ismagilov, A. D. Stroock, P. J. Kenis, G. Whitesides, H. A. Stone, *Appl. Phys. Lett.* **2000**, *76*, 2376–2378.
- [53] A. Böhm, F. Carstens, C. Trieb, S. Schabel, M. Biesalski, *Microfluid. Nanofluid.* **2014**, *16*, 789–799.
- [54] E. W. Washburn, *Phys. Rev.* **1921**, *17*, 273.
- [55] M. Reysat, L. Courbin, E. Reysat, H. A. Stone, *J. Fluid Mech.* **2008**, *615*, 335–344.
- [56] S. Mendez, E. M. Fenton, G. R. Gallegos, D. N. Petsev, S. S. Sibbett, H. A. Stone, Y. Zhang, G. P. López, *Langmuir* **2009**, *26*, 1380–1385.
- [57] J. Xiao, H. A. Stone, D. Attinger, *Langmuir* **2012**, *28*, 4208–4212.
- [58] L.-L. Shen, G.-R. Zhang, M. Biesalski, B. J. Etzold, *Lab Chip* **2019**, *19*, 3438–3447.
- [59] A. K. Yetisen, M. S. Akram, C. R. Lowe, *Lab Chip* **2013**, *13*, 2210–2251.
- [60] E. Fu, P. Kauffman, B. Lutz, P. Yager, *Sens. Actuators B* **2010**, *149*, 325–328.
- [61] E. Fu, B. Lutz, P. Kauffman, P. Yager, *Lab Chip* **2010**, *10*, 918–920.
- [62] P. Kauffman, E. Fu, B. Lutz, P. Yager, *Lab Chip* **2010**, *10*, 2614–2617.
- [63] E. Elizalde, R. Urteaga, C. L. Berli, *Lab Chip* **2015**, *15*, 2173–2180.
- [64] B. J. Toley, B. McKenzie, T. Liang, J. R. Buser, P. Yager, E. Fu, *Anal. Chem.* **2013**, *85*, 11545–11552.
- [65] Z. Nie, C. A. Nijhuis, J. Gong, X. Chen, A. Kumachev, A. W. Martinez, M. Narovlyansky, G. M. Whitesides, *Lab Chip* **2010**, *10*, 477–483.
- [66] X. Li, C. Zhao, X. Liu, *Microsyst. Nanoeng.* **2015**, *1*, 15014.
- [67] D. Zang, L. Ge, M. Yan, X. Song, J. Yu, *Chem. Commun.* **2012**, *48*, 4683–4685.
- [68] P. Wang, L. Ge, S. Ge, J. Yu, M. Yan, J. Huang, *Chem. Commun.* **2013**, *49*, 3294–3296.
- [69] L. Y. Shiroma, M. Santhiago, A. L. Gobbi, L. T. Kubota, *Anal. Chim. Acta* **2012**, *725*, 44–50.
- [70] M. Zhang, L. Ge, S. Ge, M. Yan, J. Yu, J. Huang, S. Liu, *Biosens. Bioelectron.* **2013**, *41*, 544–550.
- [71] G. Sun, P. Wang, S. Ge, L. Ge, J. Yu, M. Yan, *Biosens. Bioelectron.* **2014**, *56*, 97–103.
- [72] Z. Li, F. Li, J. Hu, W. H. Wee, Y. L. Han, B. Pingguan-Murphy, T. J. Lu, F. Xu, *Analyst* **2015**, *140*, 5526–5535.
- [73] Z. Nie, F. Deiss, X. Liu, O. Akbulut, G. M. Whitesides, *Lab Chip* **2010**, *10*, 3163–3169.
- [74] A. A. Rowe, A. J. Bonham, R. J. White, M. P. Zimmer, R. J. Yadgar, T. M. Hobza, J. W. Honea, I. Ben-Yaacov, K. W. Plaxco, *PLoS One* **2011**, *6*, e23783.
- [75] V. Beni, D. Nilsson, P. Arven, P. Norberg, G. Gustafsson, A. P. Turner, *ECS J. Solid State Sci. Technol.* **2015**, *4*, S3001–S3005.
- [76] G. G. Lewis, M. J. DiTucci, M. S. Baker, S. T. Phillips, *Lab Chip* **2012**, *12*, 2630–2633.
- [77] P. Wang, L. Ge, M. Yan, X. Song, S. Ge, J. Yu, *Biosens. Bioelectron.* **2012**, *32*, 238–243.
- [78] J. Lu, S. Ge, L. Ge, M. Yan, J. Yu, *Electrochim. Acta* **2012**, *80*, 334–341.
- [79] Y. Wu, P. Xue, Y. Kang, K. M. Hui, *Anal. Chem.* **2013**, *85*, 8661–8668.
- [80] Y. Wu, P. Xue, K. M. Hui, Y. Kang, *Biosens. Bioelectron.* **2014**, *52*, 180–187.
- [81] P. Wang, G. Sun, L. Ge, S. Ge, X. Song, M. Yan, J. Yu, *Chem. Commun.* **2013**, *49*, 10400–10402.
- [82] Y. Wang, L. Ge, P. Wang, M. Yan, S. Ge, N. Li, J. Yu, J. Huang, *Lab Chip* **2013**, *13*, 3945–3955.
- [83] J. Yan, M. Yan, L. Ge, J. Yu, S. Ge, J. Huang, *Chem. Commun.* **2013**, *49*, 1383–1385.
- [84] G. Sun, Y. Zhang, Q. Kong, C. Ma, J. Yu, S. Ge, M. Yan, X. Song, *J. Mater. Chem. B* **2014**, *2*, 7679–7684.
- [85] J. Yan, M. Yan, L. Ge, S. Ge, J. Yu, *Sens. Actuators B* **2014**, *193*, 247–254.
- [86] S. Ge, W. Li, M. Yan, X. Song, J. Yu, *J. Mater. Chem. B* **2015**, *3*, 2426–2432.
- [87] Y. Wang, H. Liu, P. Wang, J. Yu, S. Ge, M. Yan, *Sens. Actuators B* **2015**, *208*, 546–553.
- [88] S. Ge, F. Lan, L. Liang, N. Ren, L. Li, H. Liu, M. Yan, J. Yu, *ACS Appl. Mater. Interfaces* **2017**, *9*, 6670–6678.
- [89] T. Akyazi, L. Basabe-Desmonts, F. Benito-Lopez, *Anal. Chim. Acta* **2018**, *1001*, 1–17.
- [90] A. P. F. Turner, *Chem. Soc. Rev.* **2013**, *42*, 3184–3196.
- [91] E. Witkowska Nery, M. Kundys, P. S. Jeleń, M. Jönsson-Niedziółka, *Anal. Chem.* **2016**, *88*, 11271–11282.
- [92] J. Kudr, O. Zitka, M. Klimanek, R. Vrba, V. Adam, *Sens. Actuators B* **2017**, *246*, 578–590.
- [93] H. Hou, K. M. Zeinu, S. Gao, B. Liu, J. Yang, J. Hu, *Energy Environ. Mater.* **2018**, *1*, 113–131.
- [94] G. Hanrahan, D. G. Patil, J. Wang, *J. Environ. Monit.* **2004**, *6*, 657–664.
- [95] P. Apostoli, *J. Chromatogr. B* **2002**, *778*, 63–97.
- [96] R. T. Kachosangi, C. E. Banks, X. Ji, R. G. Compton, *Anal. Sci.* **2007**, *23*, 283–289.
- [97] Z. Zou, A. Jang, E. MacKnight, P.-M. Wu, J. Do, P. L. Bishop, C. H. Ahn, *Sens. Actuators B* **2008**, *134*, 18–24.
- [98] T. Florence, *J. Electroanal. Chem. Interfacial Electrochem.* **1970**, *27*, 273–281.
- [99] H. P. Wu, *Anal. Chem.* **1996**, *68*, 1639–1645.
- [100] J. Wang, J. Lu, S. B. Hocevar, P. A. Farias, B. Ogorevc, *Anal. Chem.* **2000**, *72*, 3218–3222.
- [101] J. Wang, J. Lu, Ü. A. Kirgöz, S. B. Hocevar, B. Ogorevc, *Anal. Chim. Acta* **2001**, *434*, 29–34.
- [102] G. Kefala, A. Economou, A. Voulgaropoulos, M. Sofoniou, *Talanta* **2003**, *61*, 603–610.
- [103] N. Lezi, A. Economou, P. A. Dimovasilis, P. N. Trikalitis, M. I. Prodromidis, *Anal. Chim. Acta* **2012**, *728*, 1–8.
- [104] G.-H. Hwang, W.-K. Han, J.-S. Park, S.-G. Kang, *Sens. Actuators B* **2008**, *135*, 309–316.

- [105] R. O. Kadara, I.E. Tothill, *Anal. Bioanal. Chem.* **2004**, *378*, 770–775.
- [106] R. O. Kadara, I.E. Tothill, *Anal. Chim. Acta* **2008**, *623*, 76–81.
- [107] G. Aragay, J. Pons, A. Merkoçi, *J. Mater. Chem.* **2011**, *21*, 4326–4331.
- [108] S. B. Hočevar, B. Ogorevc, J. Wang, B. Pihlar, *Electroanalysis* **2002**, *14*, 1707–1712.
- [109] A. Economou, *TrAC Trends Anal. Chem.* **2005**, *24*, 334–340.
- [110] J. Wang, *Electroanalysis* **2005**, *17*, 1341–1346.
- [111] Y. Wang, D. Zhang, S. Ge, L. Ge, J. Yu, M. Yan, *Electrochim. Acta* **2013**, *107*, 147–154.
- [112] M. Y.-C. Wu, M.-Y. Hsu, S.-J. Chen, D.-K. Hwang, T.-H. Yen, C.-M. Cheng, *Trends Biotechnol.* **2017**, *35*, 288–300.
- [113] C. S. K. Lawrence, S. N. Tan, C. Z. Floresca, *Sens. Actuators B* **2014**, *193*, 536–541.
- [114] K. B. Lee, *J. Micromech. Microeng.* **2006**, *16*, 2312–2317.
- [115] Y. Koo, J. Sankar, Y. Yun, *Biomicrofluidics* **2014**, *8*, 054104.
- [116] H. Lee, S. Choi, *Nano Energy* **2015**, *15*, 549–557.
- [117] R. K. Arun, S. Halder, N. Chanda, S. Chakraborty, *Lab Chip* **2014**, *14*, 1661–1664.
- [118] M. J. González-Guerrero, F. J. del Campo, J. P. Esquivel, F. Giroud, S. D. Minter, N. Sabaté, *J. Power Sources* **2016**, *326*, 410–416.
- [119] X. Yan, A. Xu, L. Zeng, P. Gao, T. Zhao, *Energy Technol.* **2018**, *6*, 140–143.
- [120] K. B. Lee, *J. Micromech. Microeng.* **2005**, *15*, S210–S214.
- [121] K. B. Lee, *J. Micromech. Microeng.* **2006**, *16*, 2312–2317.
- [122] H. Liu, R. M. Crooks, *Anal. Chem.* **2012**, *84*, 2528–2532.
- [123] N. K. Thom, G. G. Lewis, M. J. DiTucci, S. T. Phillips, *RSC Adv.* **2013**, *3*, 6888–6895.
- [124] X. Zhang, J. Li, C. Chen, B. Lou, L. Zhang, E. Wang, *Chem. Commun.* **2013**, *49*, 3866–3868.
- [125] Y. Zhang, L. Li, L. Zhang, S. Ge, M. Yan, J. Yu, *Nano Energy* **2017**, *31*, 174–182.
- [126] X. Wei, H. Lee, S. Choi, *Sens. Actuators B* **2016**, *228*, 151–155.
- [127] A. Fraiwan, S. Choi, *Phys. Chem. Chem. Phys.* **2014**, *16*, 26288–26293.
- [128] M. Mohammadifar, S. Choi, *Adv. Mater. Technol.* **2017**, *2*, 1700127.
- [129] O. A. Ibrahim, P. Alday, N. Sabaté, J. P. Esquivel, E. Kjeang, *J. Electrochem. Soc.* **2017**, *164*, A2448–A2456.
- [130] F. Cheng, J. Chen, *Chem. Soc. Rev.* **2012**, *41*, 2172–2192.
- [131] Y. Li, J. Lu, *ACS Energy Lett.* **2017**, *2*, 1370–1377.
- [132] N. Jayaprakash, S. K. Das, L. A. Archer, *Chem. Commun.* **2011**, *47*, 12610–12612.
- [133] D. J. Kim, D.-J. Yoo, M. T. Otley, A. Prokofjevs, C. Pezzato, M. Owczarek, S. J. Lee, J. W. Choi, J. F. Stoddart, *Nat. Energy* **2018**, *1*.
- [134] Q. Li, N. J. Bjerrum, *J. Power Sources* **2002**, *110*, 1–10.
- [135] S. Yang, H. Knickle, *J. Power Sources* **2002**, *112*, 162–173.
- [136] Y. Liu, Q. Sun, W. Li, K. R. Adair, J. Li, X. Sun, *Green Energ. Environ.* **2017**, *2*, 246–277.
- [137] Y. Wang, H. Kwok, W. Pan, H. Zhang, D. Y. Leung, *J. Power Sources* **2019**, *414*, 278–282.
- [138] Y. Bing, H. Liu, L. Zhang, D. Ghosh, J. Zhang, *Chem. Soc. Rev.* **2010**, *39*, 2184–2202.
- [139] L. Lin, Q. Zhu, A.-W. Xu, *J. Am. Chem. Soc.* **2014**, *136*, 11027–11033.
- [140] G. R. Zhang, M. Munoz, B. J. Etzold, *Angew. Chem. Int. Ed.* **2016**, *55*, 2257–2261; *Angew. Chem.* **2016**, *128*, 2298–2302.
- [141] G.-R. Zhang, T. Wolker, D. J. Sandbeck, M. Munoz, K. J. Mayrhofer, S. Cherevko, B. J. Etzold, *ACS Catal.* **2018**, *8*, 8244–8254.
- [142] G. Merle, M. Wessling, K. Nijmeijer, *J. Membr. Sci.* **2011**, *377*, 1–35.
- [143] J. R. Varcoe, P. Atanassov, D. R. Dekel, A. M. Herring, M. A. Hickner, P. A. Kohl, A. R. Kucernak, W. E. Mustain, K. Nijmeijer, K. Scott, *Energy Environ. Sci.* **2014**, *7*, 3135–3191.
- [144] I. Martinaiou, T. Wolker, A. Shahraei, G.-R. Zhang, A. Janßen, S. Wagner, N. Weidler, R. W. Stark, B. J. M. Etzold, U. I. Kramm, *J. Power Sources* **2018**, *375*, 222–232.
- [145] R. Ferrigno, A. D. Stroock, T. D. Clark, M. Mayer, G. M. Whitesides, *J. Am. Chem. Soc.* **2002**, *124*, 12930–12931.
- [146] E. R. Choban, L. J. Markoski, A. Wiecekowsk, P. J. Kenis, *J. Power Sources* **2004**, *328*, 54–60.
- [147] J. L. Cohen, D. J. Volpe, D. A. Westly, A. Pechenik, H. D. Abruña, *Langmuir* **2005**, *21*, 3544–3550.
- [148] R. S. Jayashree, L. Gancs, E. R. Choban, A. Primak, D. Natarajan, L. J. Markoski, P. J. Kenis, *J. Am. Chem. Soc.* **2005**, *127*, 16758–16759.
- [149] M.-H. Chang, F. Chen, N.-S. Fang, *J. Power Sources* **2006**, *159*, 810–816.
- [150] F. Chen, M.-H. Chang, M.-K. Lin, *Electrochim. Acta* **2007**, *52*, 2506–2514.
- [151] E. Kjeang, J. McKechnie, D. Sinton, N. Djilali, *J. Power Sources* **2007**, *168*, 379–390.
- [152] W. Sung, J.-W. Choi, *J. Power Sources* **2007**, *172*, 198–208.
- [153] E. Kjeang, R. Michel, D. A. Harrington, N. Djilali, D. Sinton, *J. Am. Chem. Soc.* **2008**, *130*, 4000–4006.
- [154] F. R. Brushett, R. S. Jayashree, W.-P. Zhou, P. J. Kenis, *Electrochim. Acta* **2009**, *54*, 7099–7105.
- [155] D. Morales-Acosta, L. A. Godinez, L. Arriaga, *J. Power Sources* **2010**, *195*, 1862–1865.
- [156] M. R. Thorson, F. R. Brushett, C. J. Timberg, P. J. Kenis, *J. Power Sources* **2012**, *218*, 28–33.
- [157] M. J. González-Guerrero, J. P. Esquivel, D. Sánchez-Molas, P. Godignon, F. X. Muñoz, F. J. Del Campo, F. Giroud, S. D. Minter, N. Sabaté, *Lab Chip* **2013**, *13*, 2972–2979.
- [158] T. S. Copenhaver, K. H. Purohit, K. Domalaon, L. Pham, B. J. Burgess, N. Manorothkul, V. Galvan, S. Sotez, F. A. Gomez, J. L. Haan, *Electrophoresis* **2015**, *36*, 1825–1829.
- [159] V. Galvan, K. Domalaon, C. Tang, S. Sotez, A. Mendez, M. Jalali-Heravi, K. Purohit, L. Pham, J. Haan, F. A. Gomez, *Electrophoresis* **2016**, *37*, 504–510.
- [160] S. Calabrese Barton, J. Gallaway, P. Atanassov, *Chem. Rev.* **2004**, *104*, 4867–4886.
- [161] T. Miyake, K. Haneda, N. Nagai, Y. Yatagawa, H. Onami, S. Yoshino, T. Abe, M. Nishizawa, *Energy Environ. Sci.* **2011**, *4*, 5008–5012.
- [162] C. W. N. Villarrubia, C. Lau, G. P. Ciniciato, S. O. Garcia, S. S. Sibbett, D. N. Petsev, S. Babanova, G. Gupta, P. Atanassov, *Electrochem. Commun.* **2014**, *45*, 44–47.

Manuscript received: September 10, 2019  
 Revised manuscript received: October 31, 2019  
 Accepted manuscript online: November 4, 2019